REALIZATION OF MICROFLUIDIC DEVICES WITH STEEL DISPLACEMENT AMPLIFIERS FOR CELL CULTURING AND ANALYSIS

by

Emre İşeri

B.S., Electrical and Electronics Engineering, Boğaziçi University, 2013

Submitted to the Institute for Graduate Studies in
Science and Engineering in partial fulfillment of
the requirements for the degree of
Master of Science

Graduate Program in Electrical and Electronics Engineering
Boğaziçi University
2015

ACKNOWLEDGEMENTS

I would like to express my gratitude to people who have contributed to this work and have made this thesis possible.

Family comes first. Their endless support always encourages me throughout my life. I am greatful to my parents, my little brother and my cousins. They made me a person who I am now and I have a lot to learn from them. I now they will always stand by me and I cannot describe how lucky I am to have such a family.

My supervisor, Prof. Şenol Mutlu gave me an opportunity to work with him. He showed me how to become a multidisciplinary person and how to produce innovative ideas and creative solutions. His original ideas and suggestions made this thesis possible. Here I would like to thank him for all. It is pleasure to work with him. I also want to thank Prof. Kutlu Ülgen and Prof. Çetin Yılmaz. They are the sources of inspiration of this study. Their valuable contributions and ideas constructed the keystones of this thesis.

There are some dearest people that I would like to mention here. I am thankful to Burcu for her precious friendship since 2009. It could not be possible to finish this thesis in time without her support. I am delighted to work with Ozan in the same lab. He is the best friend that I met in last two years. And I am also greatful to Gözde for her sincere friendship.

The BETA family; I thank you all. I would like to thank Gürkan Sönmez who shared his priceless experiences and knowledge, Engin Afacan and Gönenç Berkol who patiently endured my all trollings, İskender Haydaroğlu who did not beat me due to my saucy jokes. In addition, a sincere gratitude goes to Okan Zafer Batur for his entertaining argues with me and Feyyaz Melih Akçakaya, İsmail Kara, Berk Çamlı, and Hikmet Çeliker for their close friendship. I also would like to thank İlhan Yıldırım as an honorary member of BETA family. Finally, I would like to thank Dağhan

Gökdel, Baykal Sarıoğlu, Orhan Mert and other elder members of BETA family for their heritage of wonderful fund of knowledge and experiences.

This work is supported by Bogazici University Research Fund under Grant 7082S and 7901R.

ABSTRACT

REALIZATION OF MICROFLUIDIC DEVICES WITH STEEL DISPLACEMENT AMPLIFIERS FOR CELL CULTURING AND ANALYSIS

In this thesis, microfluidic devices with simple trapping mechanism which can be actuated by applying force to use them for cell culturing and analysis applications are designed, analyzed and fabricated. Steel displacement amplifiers are designed, analytically evaluated and simulated to use them as trapping mechanism in microfluidic channels. In addition, analytical model of the hydrodynamic resistance of device and the results of the flow simulations are discussed in order to describe and characterize the device. 50μm-thick steel thin films, 1 mm-thick Poly methyl methacrylate (PMMA) plates, and 125μm-thick Polyethylene naphthalate (PEN) films are used to realize the device. Fabrication methods, which are photolitography, electrochemical etching, wet etching, hot embossing, thermo-compression bonding and laser micromachining are illustrated. Electrochemical etching process is characterized. Results of displacement measurements of the steel displacement amplifier under different loads is presented . Coefficient of thermal expansion (CTE) difference problem that is encountered during hot embossing process of steel and PMMA is discussed. It is shown that using PEN substrates which have almost same CTE as the steel thin films solve the CTE mismatch issue. In conclusion, the final version of the fabricated device is presented. Moreover, necessary studies in order to actuate steel displacement amplifier embedded in microfluidic channel are discussed as a future work.

ÖZET

HÜCRE KÜLTÜRLEME VE ANALİZİ İÇİN ÇELİK YERDEĞİŞTİRME YÜKSELTEÇLİ MİKROAKIŞKAN CİHAZLARIN GERÇEKLEŞTİRİLMESİ

Bu tezde hücre kültürleme ve analiz uygulamaları için kuvvet uygulayarak hareket ettirilebilen basit tuzak mekanizmalı mikroakışkan cihazlar tasarlanmıştır ve bu cihazların analiz ve üretimi yapılmıştır. Mikroakışkan kanallar içinde basit tuzak mekanizması olarak kullanılması amacı ile çelik yerdeğiştirme yükselteçleri tasarlanmış, analitik olarak değerlendirilmiş ve benzetimleri yapılmıştır. Ayrıca cihazın tanımlanması ve karakterizasyonunun yapılması amacı ile hidrodinamik direnç modellemesi ve akış benzetimi sonuçları tartışılmıştır. Cihazın gerçekleştirilmesi için 50μm kalınlığında çelik ince filmler, 1 mm kalınlığında PMMA levhalar ve 125μm kalınlığında PEN filmler kullanılmıştır. Fabrikasyonda kullanılan fotolitografi, elektrokimyasal aşındırma, kimyasal aşındırma, sıcak gofraj, termo-kompresyon birleştirme ve lazer mikroimalat yöntemleri gösterilmiştir. Elektrokimyasal aşındırma süreci karakterize edilmiştir. Çelik yerdeğiştirme yükseltecinin farklı yükler altında yapılmış olan yerdeğiştirme ölçümlerinin sonuçları sunulmuştur. Farklı ısıl genleşme katsayıları nedeni ile PMMA ve çeliğin sıcak gofrajı sırasında karşılaşılan problemler tartışılmıştır. Bu sorunun ısıl genleşme katsayısı çelik ile neredeyse aynı olan PEN substratlar kullanılarak aşılabileceği gösterilmiştir. Sonuç olarak üretilen cihazların son sürümü sunulmuştur. Buna ek olarak mikroakışkan kanal içine gömülmüş çelik yükseltecin hareket ettirilebilmesi için gereken çalışmalar ileride yapılmak üzere tartışılmıştır.

TABLE OF CONTENTS

LIST OF FIGURES

LIST OF TABLES

LIST OF SYMBOLS

A	Cross-sectional area
A_1	Cross-sectional area of R_1
A_2	Cross-sectional area of R_2
C_2H_6O	Ethanol
$CHCl_3$	Chloroform
E	Young's modulus of elasticity
F	Force
H_2O	Water
HCl	Hydrochloric acid
HNO_3	Nitric acid
h_1	Height of the cross-sectional area A_1
h_2	Height of the cross-sectional area A_2
h_c	Height of the microfluidic channel
h_c	Height of the valve
I	Electrical current
k_a	Spring constant between m_a and other mass
L	Length of the microfluidic channel
L_0	Initial length
L_in	Length of the inlet
L_out	Length of the outlet
L_valve	Length of the valve
$NaCl$	Sodium chloride
Q	Flow rate (volume)
R	Electrical resistance / resistor
R_1	Hydrodynamic resistance of the cross-sectional region A_1
R_2	Hydrodynamic resistance of the cross-sectional region A_2
R_h	Hydrodynamic resistance
R_in	Hydrodynamic resistance of the inlet

R_{out}	Hydrodynamic resistance of the outlet
R_{valve}	Hydrodynamic resistance of the valve
V	Electrical potential difference (voltage)
W	Width of the microfluidic channel
W_1	Width of the opening between valve and channel
W_2	Width of the valve in channel
x_1	Displacement of $m^{'}$ in x-direction
x_2	Displacement of $m^{''}$ in x-direction
z_1	Displacement of m_{a} in x-direction
z_2	Displacement of m_{a} in y-direction
α_{L}	Linear coefficient of thermal expansion
α_{p}	Linear coefficient of thermal expansion of the PMMA
α_{s}	Linear coefficient of thermal expansion of the steel
δL	Change in the length due to thermal expansion
δL_{p}	Change in the length of the PMMA due to thermal expansion
δL_{s}	Change in the length of the steel due to thermal expansion
δT	Temperature difference
δx	Displacement in x-direction
δy	Displacement in y-direction
μ	Dynamic viscosity
θ	Angle of the spring

LIST OF ACRONYMS/ABBREVIATIONS

3D	Three-dimensional
AISI	American Iron and Steel Institute
CAD	Computer aided design
CE	Capillary electrophoresis
CTE	Coefficient of thermal expansion
DI	Deionized (water)
DNA	Deoxyribonucleic acid
FEM	Finite element modeling
IPA	Isopropyl alcohol
MEMS	Micro-electro-mechanical systems
PEN	Polyethylene naphthalate
PMMA	Poly methyl methacrylate
PR	Photoresist
SMA	Shape memory alloy
UV	Ultraviolet
μTAS	Micro total analysis systems

1. INTRODUCTION

Microfluidics is an interdisciplinary field of science and technology which deals with manipulating fluids in micro or even nano scaled channels. With the studies started in early 1990s, microfluidics has become an inspiring research field for life sciences. With the first applications of microfluidics, a novel concept which is called "Micro Total Analysis Systems" (μTAS) was born. It offers faster and cheaper solutions for analysis in chemistry and biology with the advantage of using small reagent volumes [1].

Increasing needs in molecular analysis, molecular biology and genetics research are significant motivational forces for development of microfluidic technologies [2]. In addition, well known micro-electro-mechanical systems (MEMS) fabrication techniques are easily applicable for realization of microfluidic devices [3]. This provides rapid advancement and industrialization of microfluidics. Demands of biotechnology, diagnostics and medical industries have been increasing the speed of development of this technology and thousands of researchers and scientists have been spending their time on these developments [4].

1.1. Fundamentals and Applications of Microfluidics

Miniaturization of chemical and biochemical analysis systems extends the capability of devices, decreases the time consumption and the cost with high-throughput processing and analysis methods. Thus, new technology field called 'lab-on-a-chip' came up to offer many applications in drug discovery, diagnostics, chemical reactions or biological analysis [5]. Certainly, miniaturizing of these systems in a chip brings many kinds of functional elements containing mixers, valves, pumps, sensors, separators, heaters, etc. [6]. Hence, researchers started to create new configurations of these elements in a single chip to succeed analysis and synthesis systems for different applications like shown in Figure 1.1.

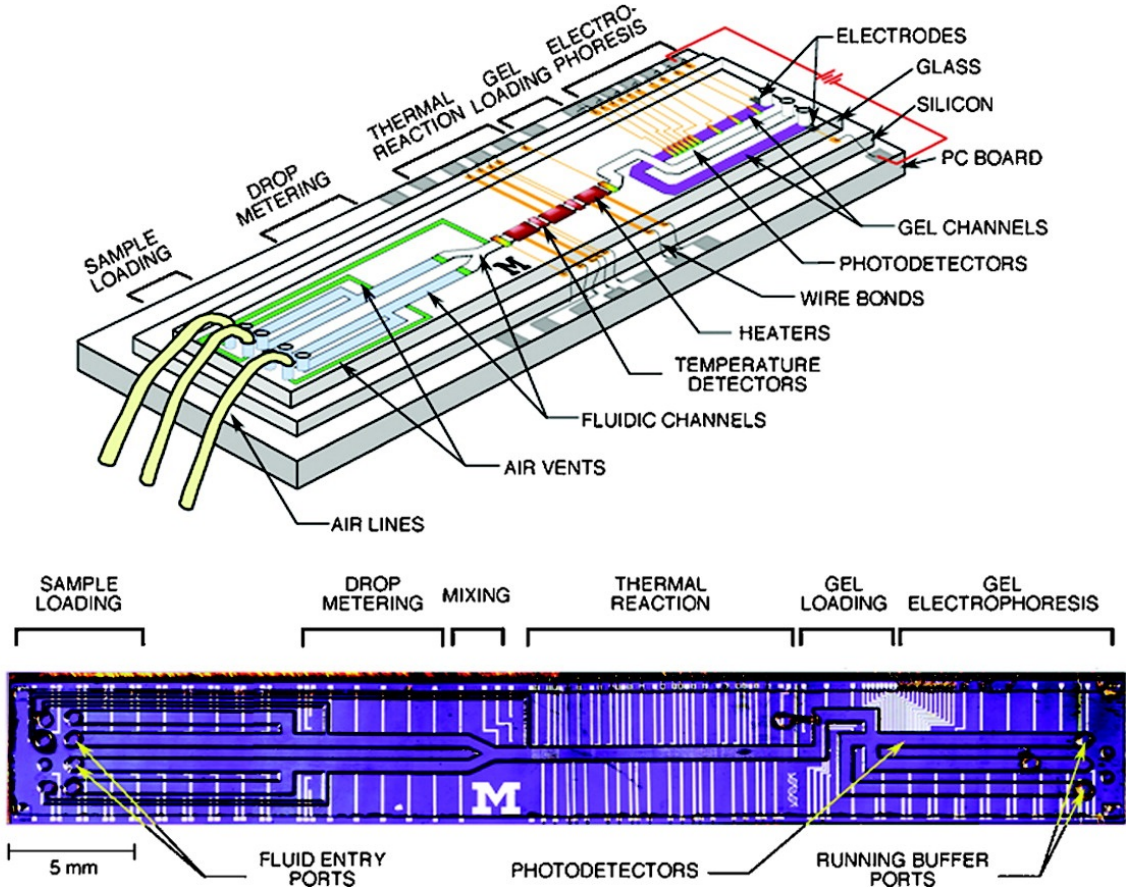

Figure 1.1. Schematic of an integrated DNA analysis device with different functional microfluidic components [7].

With using capillary electrophoresis (CE) methods, which are electrokinetic separation methods achieved in microfluidic channels on a chip [8], research on amino acids [9], proteins [10], deoxyribonucleic acids (DNAs) [7, 11–13] in microfluidic systems were accelerated. Moreover, since 2000s, researchers and scientists have started to study on more complicated structures to investigate living cells or organisms in these microsystems [14]. Interested in cell sampling, trapping, sorting and analysis systems created demands to use complex MEMS fabrication techniques. Figure 1.2 shows a silicon microteeth device integrated with 20 microns wide microfluidic channel to deform red blood cells, developed in Sandia National Laboratories. Integrating MEMS sensors and structures into fluidic components [15] has been meeting these requirements since the beginning of these research.

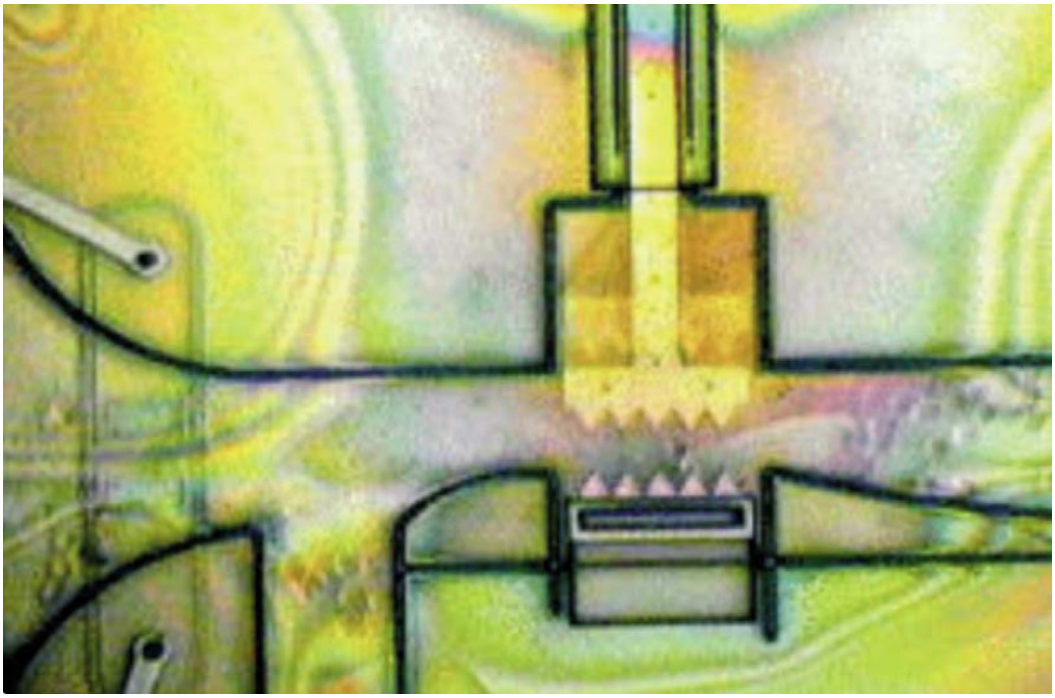

Figure 1.2. A silicon microteeth device integrated with 20 microns wide to deform red blood cells [16].

Micro valves are fundamental structures that are used for cell or particle manipulation in microfluidic channels. Several control methods were developed to realize them. One of the most popular control methods is pneumatic actuation firstly described by Quakes's group [17, 18]. There are also electromagnetically [19–21], electrostatically [22–24], thermally [25, 26], piezoelectrically [27–29] actuated valves used in

different applications. Besides with these types of microfluidic valves, creative studies like ultrasonically actuated valves [30], shape memory alloy (SMA) valves [31], and torque actuated valves [32] can be found in the literature. In Figure 1.3, several types of micro valves are illustrated. Most of these micro valves have multilayer flexible membrane structures which need complex MEMS fabrication methods to realize them.

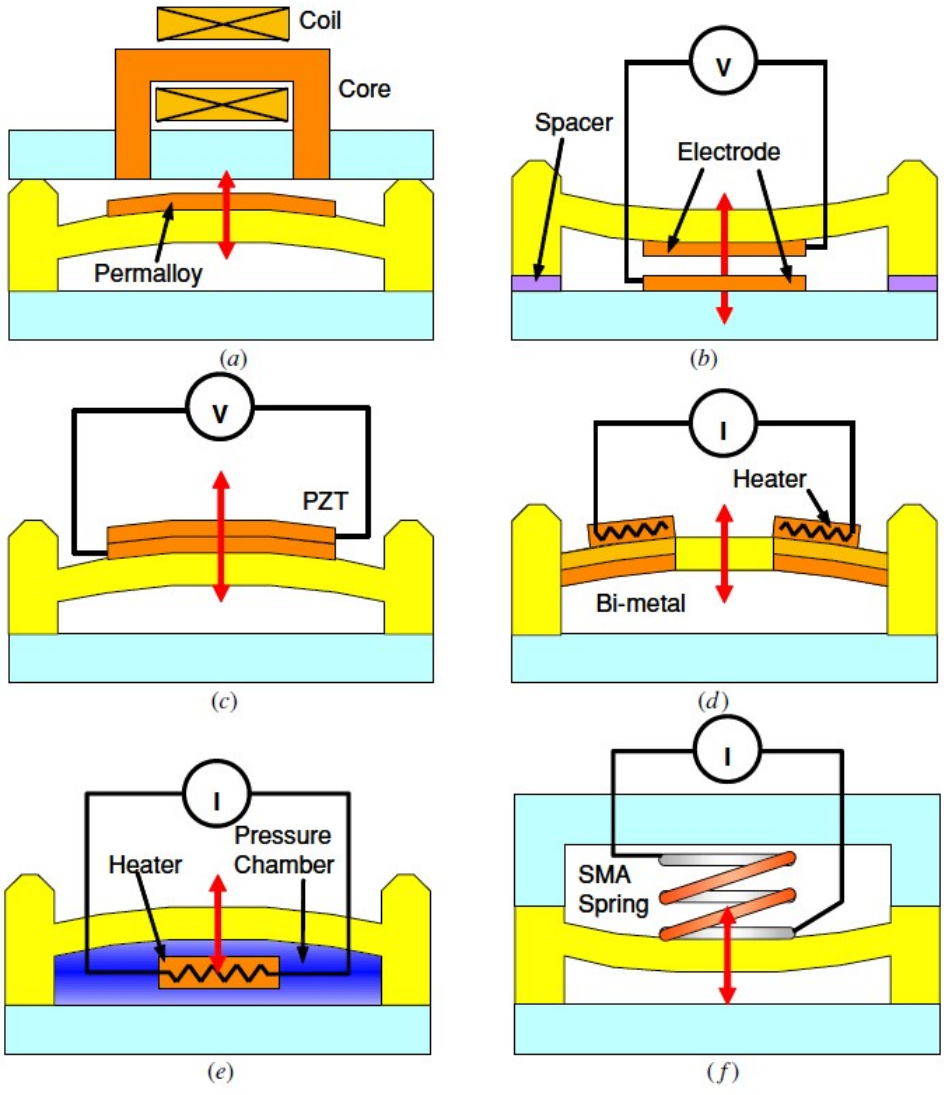

Figure 1.3. Illustration of (a)electromagnetical, (b)electrostatical, (c)piezoelectrical, (d)thermal, (e)thermo-pneumatical, and (f) shape memory alloy (SMA) based actuation of microvalves [33].

1.2. Motivation of the Thesis

As briefly reviewed in the previous part, there are many researches continue to develop microfluidic devices for different applications, since 1990s. Furthermore, industrialization in this field is rapidly going on. The studies in this field provide robust, cheap and, time saving solutions for different areas of applications.

This thesis focuses on fabricating microfluidic devices with simple trapping mechanism to use them for cell culturing and analysis applications. As mentioned in the previous section, there are many microfluidic devices developed for sampling, sorting and trapping of cells. Many of these devices require complex fabrication methods or large and expensive external equipment for micro-actuation. The motivation of this study is to produce a simple and easy mechanism to manipulate cells in a microfluidic channel, which can be used in many different applications of biochemistry and the biology. To achieve this goal, compliant displacement amplification mechanism which provides ease of usage with actuation by simple force is used. Because the compliant mechanisms are single piece structures and there is no assembly needed, using them in microfluidic channels does not need complex fabrication methods. In addition, steel is used as material to realize them due to its mechanical properties. The integration of steel compliant mechanisms in microfluidic channels can be used to develop devices for different areas of applications. Steel in microfluidic channel can also be used as electrode. As a result, this work provides novel approaches for new applications in this research area, which constitutes the main motivation of this thesis.

2. SYSTEM DESCRIPTION

In this thesis, a simple mechanical trapping mechanism inside a microfluidic channel actuated by an external mechanical force is realized for biology and cell analysis applications. Unlike the other types of microfluidic devices, this device does not require an external transducer or a complex mechanism for operation. Basic concepts of compliant mechanisms are used to actuate this device by hand or by a simple mechanical tool. Due to its proper mechanical properties, steel is used for fabricating the displacement amplifier. Poly methyl methacrylate (PMMA) is used to create microfluidic channel on it, since it is one of the typically used material to fabricate microfluidic channels and there are many studies [34–36] that shows the fabrication techniques and useful information. Total system comprised of steel fingers attached to a compliant displacement amplification mechanism which is integrated to a microfluidic channel embossed on PMMA substrates shown in Figure 2.1.

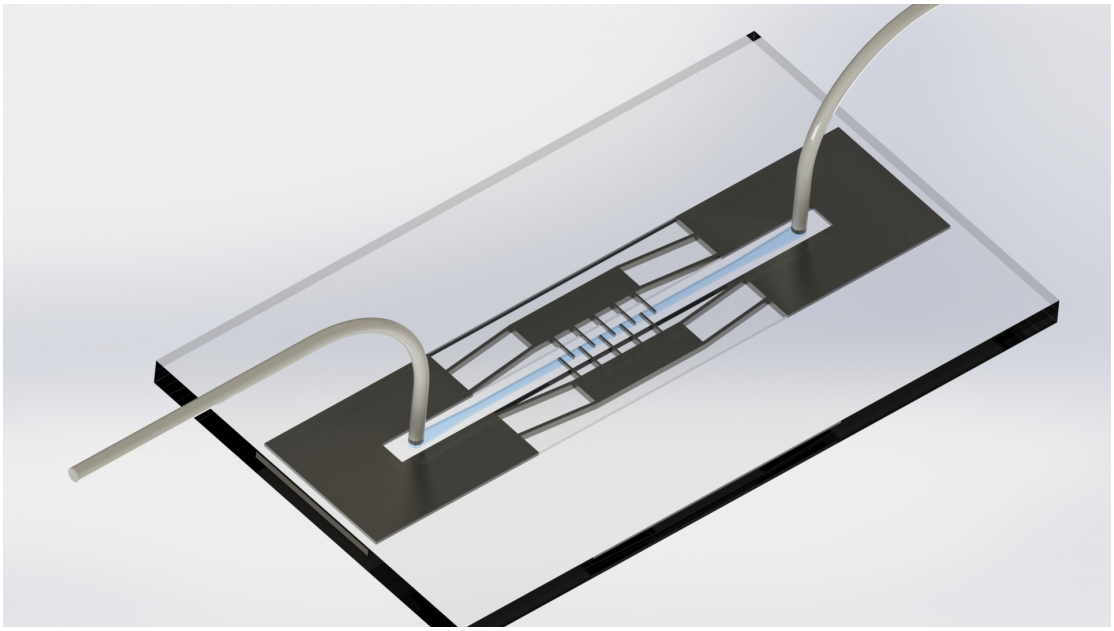

Figure 2.1. Microfluidic device with the integrated displacement amplification mechanism.

The main goal of fabricating this device is to trap, feed, and finally release and collect cells. This type of cell manipulation provides opportunity to use this device

easily in many different applications of biology and cellomics. Operation of the device is illustrated in Figure 2.2.

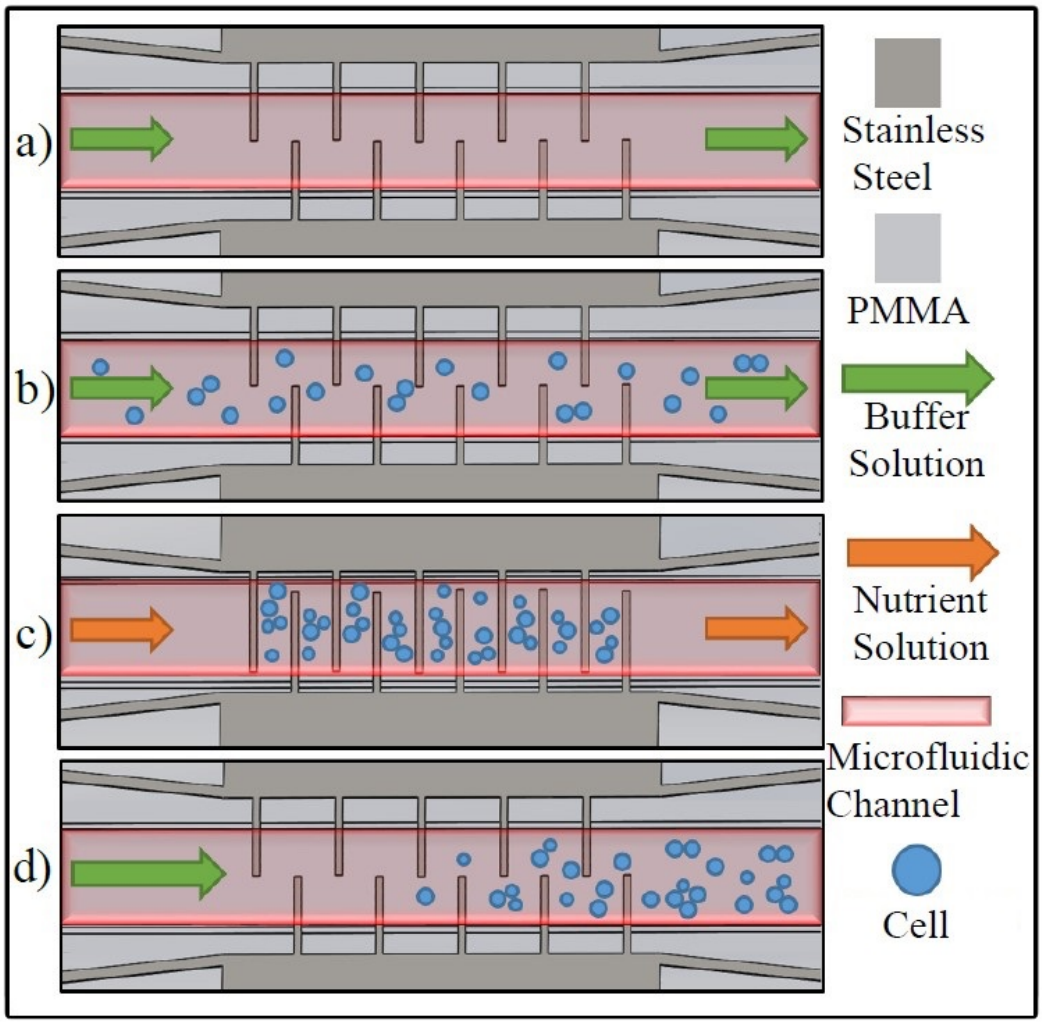

Figure 2.2. Principle operations of the device: (a) Degassing and cleaning channel, (b) loading cells, (c) cell trapping and growth, (d) unloading cells.

2.1. Displacement Amplification Mechanism

Compliant mechanisms are flexible structures that are used to transfer and/or amplify forces or displacements applied on it. There are many known compliant mechanism topologies which are revealed by mechanical engineers. Many of these can easily be used in MEMS to offer practical solutions due to their assembly-free and single piece structures [37]. For this reason, using compliant displacement amplification mechanism in microfluidic device as a trapping mechanism provides operational advantages

without using any external transducer or complex instrument. There are several known topologies already realized for macro scale that can be used for this purpose [38–40].

2.1.1. Principle of Operation

A simple displacement amplification mechanism as shown in Figure 2.3 can be used for changing the direction of the displacement, and amplifying it with respect to the angle θ. x_1 and x_2 denote the displacements of m' and m'', whereas z_1 and z_2 denote the horizontal and vertical displacements of the m_a. If it is assumed that springs with stiffness k_a are rigid, the horizontal and the vertical displacements of m_a can be derived as

$$z_1 = (x_1 + x_2)/2, \tag{2.1}$$

$$z_2 = \cot(\theta)(x_1 - x_2)/2. \tag{2.2}$$

Equation 2.2 shows that displacement amplification factor is $\cot(\theta)/2$.

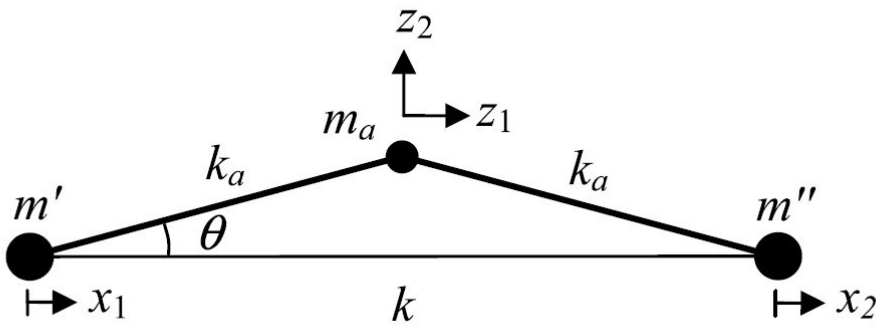

Figure 2.3. A simple displacement amplification mechanism.

Displacement amplifiers designed with finger-shaped structures is shown in Figure 2.4. As shown in Figure 2.4a, applied force causes displacement, and Δx and parallel beams transfer this displacement to the y-axis. They also amplify displacement by a factor of $\cot(\theta)/2$. There are two parallel beams for every connection which guarantee that displacement is transferred perpendicularly without any angle devia-

tion. Design in Figure 2.4b is the same as Figure 2.4a, except that the direction of the transferred displacement is reversed. They can be used in normally-on or normally-off microfluidic devices according to their applications.

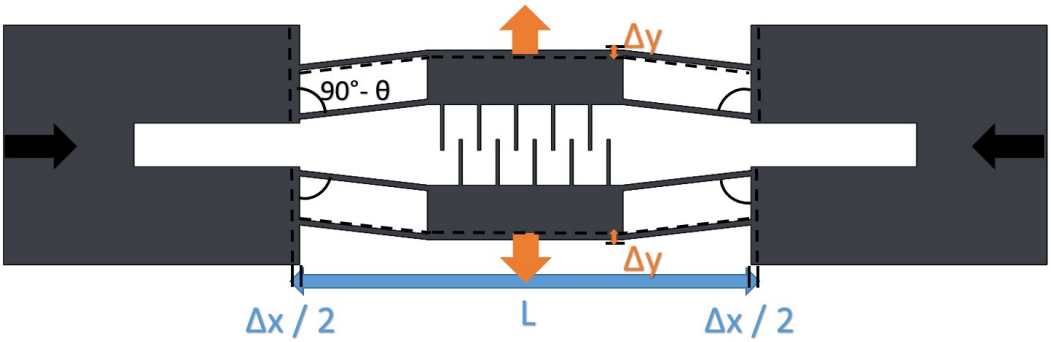

(a)

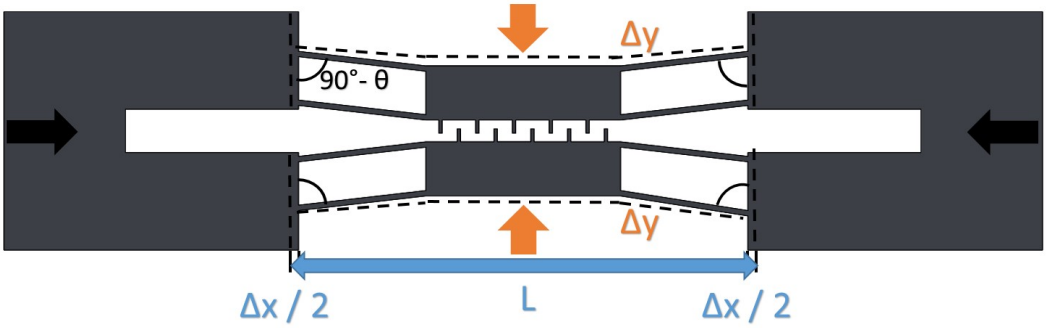

(b)

Figure 2.4. (a) Normally-off and (b) normally-on displacement amplifiers designed with finger-shaped structures.

Steel thin device integrated between two PMMA plates is shown in Figure 2.5. Steel is embedded in the two ends of the PMMA plates, whereas in the suspension region, it is free to move. Force can be applied on short edges of PMMA to actuate the steel device. Steel device is much thinner than the PMMA plates so it can be ignored when elastic displacement of the device is calculated under an applied force. In this situation, displacement Δx depends on the following formula

$$\Delta x = \frac{FL}{EA}, \tag{2.3}$$

Where F, E, A and, L denote the applied force, Young's modulus of PMMA plates, the cross sectional area of the PMMA plates, and the length of PMMA plates, respectively.

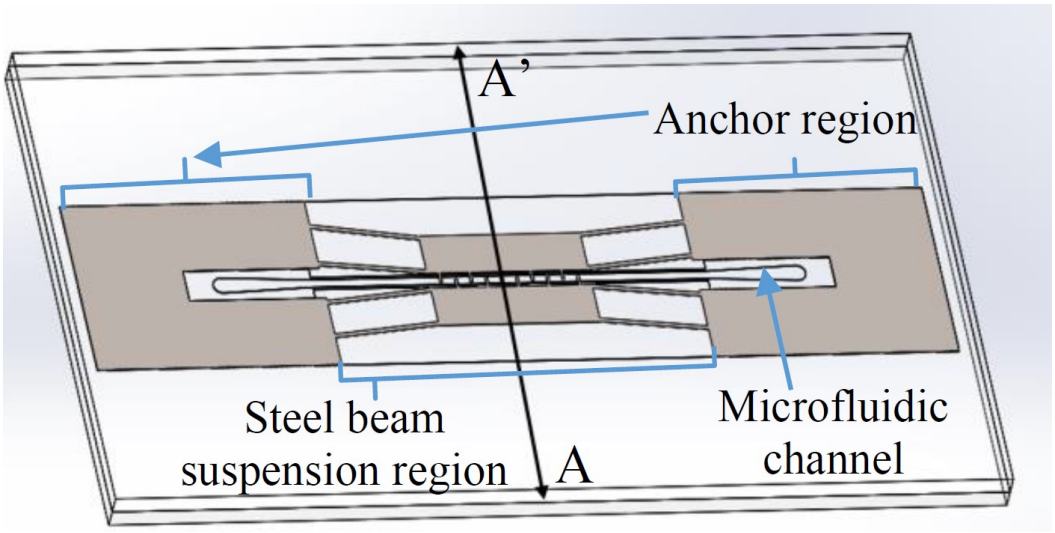

Figure 2.5. Steel thin device integrated between two PMMA plates.

Figure 2.6 shows applied force F, displacement Δy relation for different values of angle θ where $E = 3\,\text{GPa}$, $A = 60\,\text{mm}^2$, and $L = 50\,\text{mm}$.

2.1.2. Static Simulations of Displacement Amplifiers

In this section, results of static simulations of the device with specific parameters are discussed. Solidworks 2013 is used as a computer aided design (CAD) tool for simulating displacement and stress of device under an applied force. There are three parts drawn according to dimensions given in the previous section and θ is chosen as $9.46\,^\circ$. PMMA is chosen as a material for the top and the bottom parts and the American Iron and Steel Institute (AISI) 304 stainless steel is chosen as the material for the thin part in the middle.

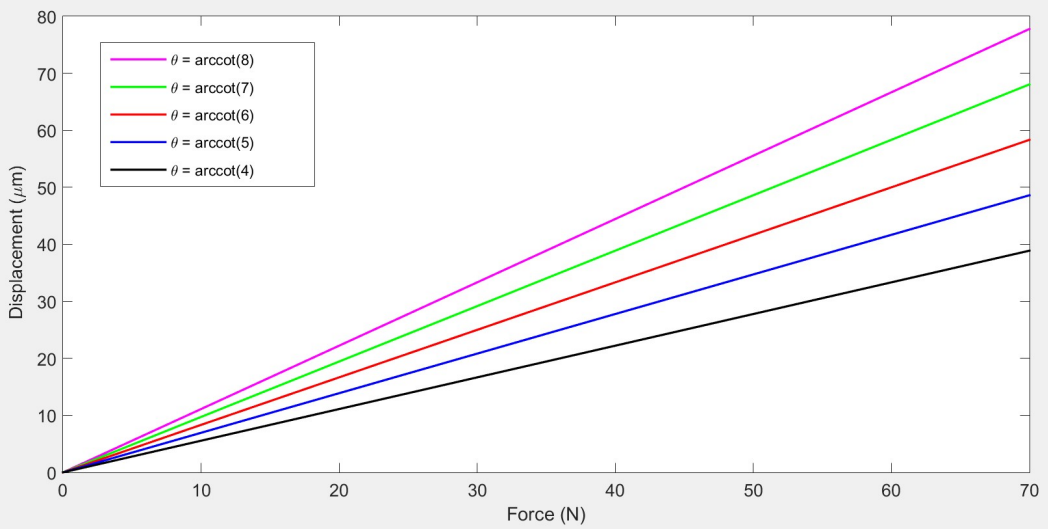

Figure 2.6. Applied force F, displacement Δy relation for different values of angle θ where $E = 3\,\text{GPa}$, $A = 60\,\text{mm}^2$, and $L = 50\,\text{mm}$.

One of the most significant parts for getting correct results from these simulations is defining right connection type for touched surfaces of the parts. Otherwise, unexpected results or errors can be encountered. For this reason, in these simulations 93 contact sets are defined as "bonded" or "no penetration" one by one according to design illustrated in Figure 2.5. The other important part is creating proper mesh which is necessary for getting accurate results. Due to the fact that the steel part is much thinner (50μm) than PMMA parts (1 mm), and there are smaller features around the microfluidic channels and steel fingers, choosing a finer mesh is needed. Also selecting "remesh failed parts with incompatible mesh" option should be on.

After defining contacts and creating the mesh, several simulations were done for different applied forces. Resultant displacement of the device under 100 N force is shown in Figure 2.7.

Figure 2.8 shows the displacement in x and y directions. As shown in Figure 2.8a, the maximum displacement in x direction is about 28μm. Only the displacement in suspension region where the parallel beams can freely move and transfer the displacement is transferred and amplified with the displacement amplification factor, $\cot(\theta)/2$. Displacement in x direction between the two edges of the suspension re-

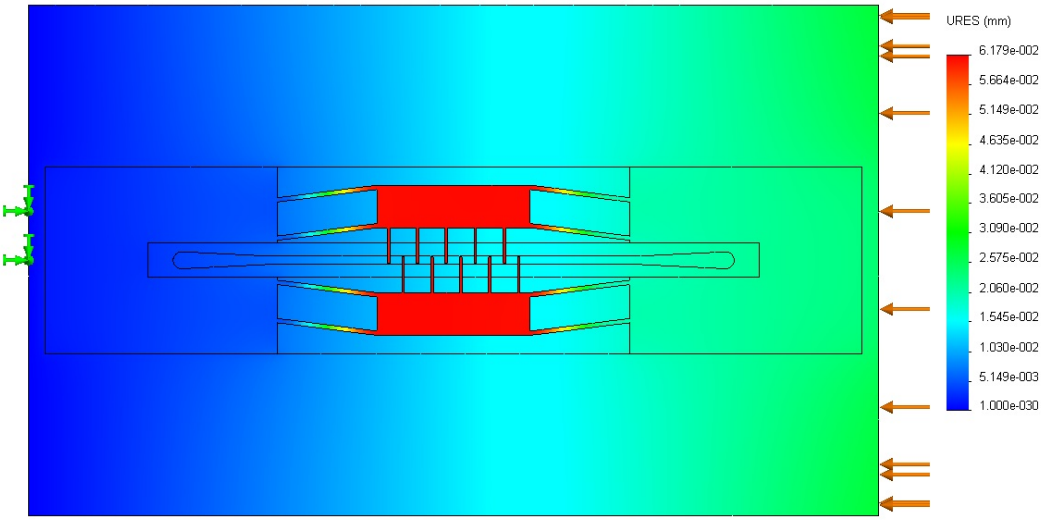

Figure 2.7. Resultant displacement of the device under 100 N force.

gion is nearly 19μm. On the other hand, the maximum displacement in y direction is 60μm. Displacement amplification factor for this design is 3 which shows the results of displacement simulations fit in with the theoretically expected values.

Yield strength is defined as stress at which plastic deformation begins. It means that irreversible deformations start above this point. Therefore, stress on the material has to stay lower than its yield strength for repeatable operation of the device. In Figure 2.9, result of von Mises stress simulation under the load of 100 N is shown. Stress is concentrated on steel part of the design due to thin structure of steel and there is almost no stress on PMMA plates. The maximum stress appears on the parallel beams and it reaches to 246 MPa. The yield strength of the stainless steel that can be used to realize this device varies between 200 MPa to 300 MPa. Thus, it can be said that applied force has to stay below 100 N for repeatable operations without plastic deformation.

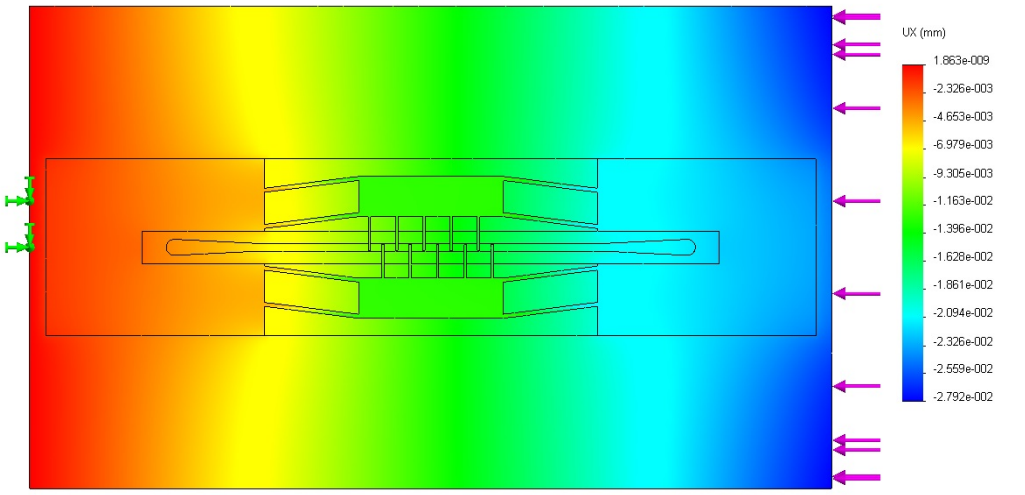

(a)

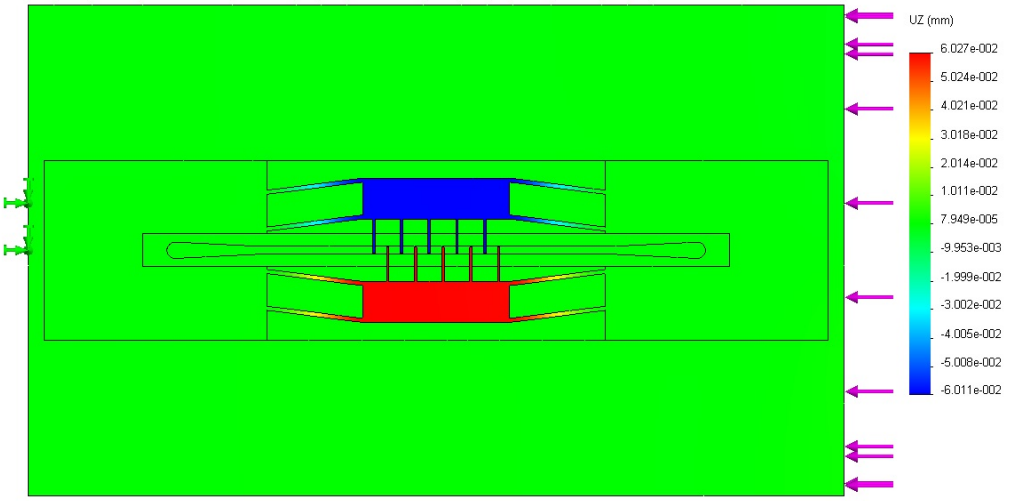

(b)

Figure 2.8. Displacement in (a) x and (b) y directions.

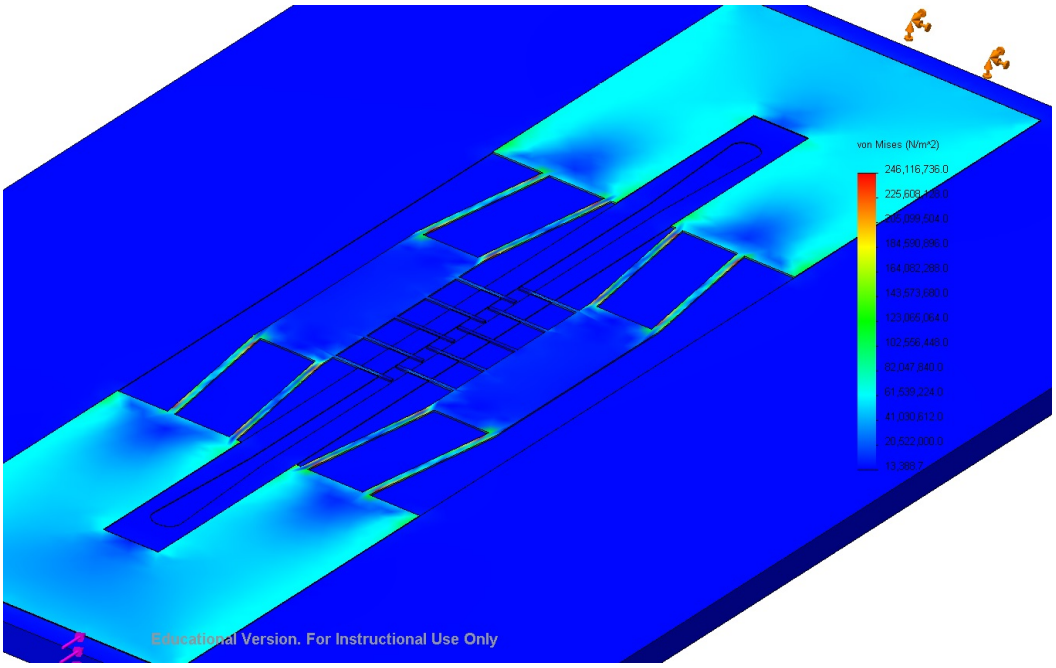

Figure 2.9. Result of von Mises stress simulation under the load of 100 N.

2.2. Microfluidic Channel Simulations of the Integrated Device

In this section, modelling of the hydrodynamic resistance of the microfluidic channel with finger shaped valves is discussed. Also the results of the flow simulation of this device are demonstrated.

2.2.1. Hydrodynamic Resistance Modelling of the Device

In fluid mechanics, Navier-Stokes equations are the most useful equations to explain many fluid dynamics related phenomenon . These equations describe the motion of fluids. Hagen-Poiseuille equations, which are one of the important and useful solutions of Navier-Stokes equations, can be used to calculate the hydrodynamic resistance of the microfluidic channels. For a channel with rectangular shaped cross section, following formula can be used to calculate hydrodynamic resistance, R_h, of the channel

$$R_h = 12\frac{\mu L}{W h^3}, \tag{2.4}$$

where μ, L, W and, h denote the dynamic viscosity, the length of the channel, the width of the channel, and the height of the channel, respectively. This formula is valid if the height of the channel is shorter than the width of the channel.

Hydrodynamic resistance can easily be related with the electrical resistance analogically. According to Ohm's Law

$$V = IR, \tag{2.5}$$

where V, I, and R denote the electric potential difference (voltage), the electrical current, and the electrical resistance, respectively. Similarly, in fluid mechanics

$$\Delta P = QR_h, \tag{2.6}$$

where ΔP and Q denote the pressure difference, and the flow rate, respectively. Thus, hydrodynamic resistances of a microfluidic device can simply be modelled like an electrical circuitry.

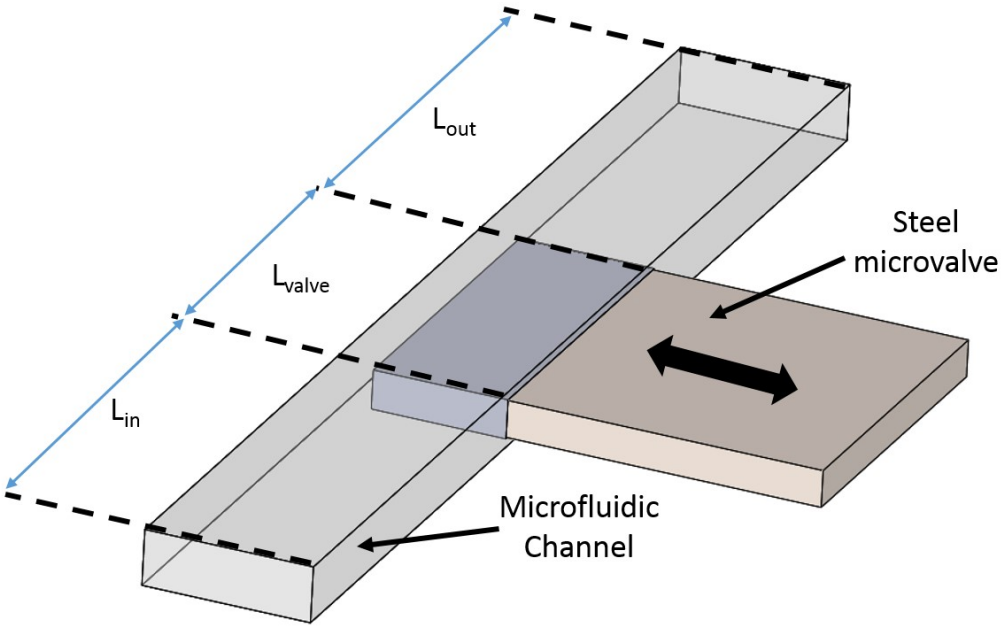

Figure 2.10. The part of the microfluidic device with valve which is free to move in perpendicular direction of the channel.

In Figure 2.10, the part of the microfluidic device with valve which is free to move in perpendicular direction of the channel is shown. There is a gap below the valve which cannot be closed with the motion of the valve. The hydrodynamic resistance of this device can be modelled as three resistances connected in series, R_{in}, R_{out} and, R_{valve}. R_{in} and R_{out} have simple rectangular cross sections and their resistance can be calculated with using (2.4) On the other hand, the resistance of the part of the channel which intersects with valve should be divided into two parts to calculate. Electrical circuit model of the device is shown in Figure 2.11.

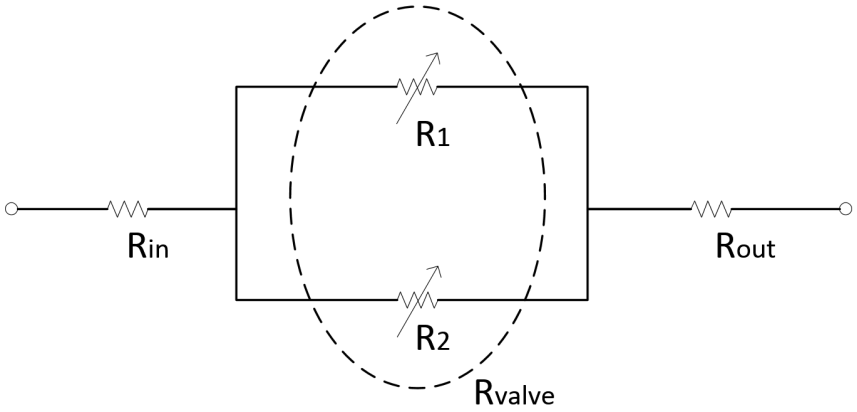

Figure 2.11. Electrical Circuit Model of the Device.

As shown in Figure 2.12, it can be thought as two cross sectional areas, A_1 and A_2, which can be modeled as two resistances connected in parallel, R_1 and R_2, respectively. Since the areas A_1 and A_2 change with the motion of the valve and the equation is valid when the channel height is lower than the channel width, this model should be dynamic. The directions of the widths and heights of the cross sectional areas were changed with respect to displacement of the valve. The dimensions used for calculating the resistances R_1 and R_2 with using (2.4) for different position intervals of the valve is given in Table 2.1.

When valve slides from fully closed position, R_2 is much smaller than R_1 at the very beginning of the motion, and decreasing the width of the A_2 causes an increase in the total resistance, which is meaningless. For that reason, at the beginning of the motion, intersection area of A_1 and A_2 shown in Figure 2.12a is considered for calculations of

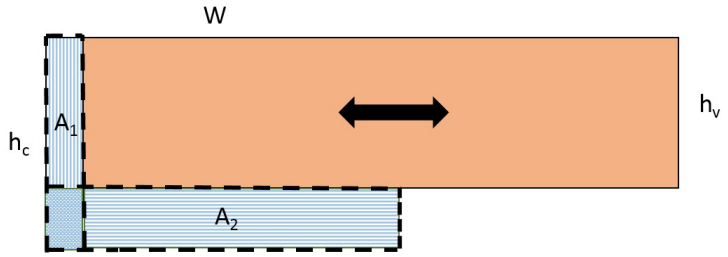

(a)

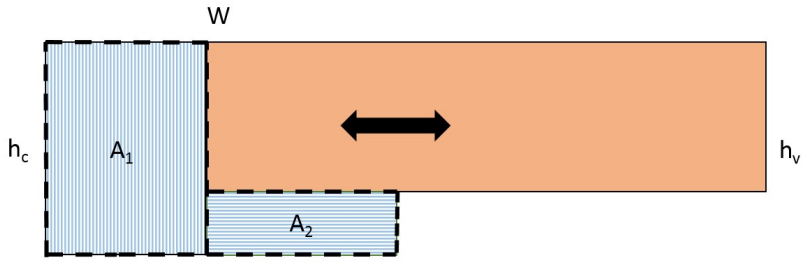

(b)

Figure 2.12. Illustration of the cross sectional areas of the hydrodynamic resistance model for (a) $\Delta x < h_c$ and (b) $\Delta x > h_c$.

Table 2.1. Dimensions that used to calculate hydrodynamic resistances R_1 and R_2 for different position intervals of the valve.

Δx	W_1	h_1	W_2	h_2
$0 - h_c$	h_c	Δx	W	$h_c - h_v$
$h_c - (W - (h_c - h_v))$	Δx	h_c	$W - \Delta x$	$h_c - h_v$
$(W - (h_c - h_v)) - W$	Δx	h_c	$h_c - h_v$	$W - \Delta x$

both resistances. After a point where R_1 becomes much smaller than R_2, which means it becomes a more dominant component for equivalent resistances, areas A_1 and A_2 shown in Figure 2.12b are considered for calculations.

Analytical model was solved in MATLAB for valve sliding from fully closed to fully opened position where $L_{in} = 400\mu$m, $L_{out} = 400\mu$m, $L_{valve} = 300\mu$m, $W_c = 240\mu$m, $h_c = 50\mu$m, and $h_v = 40\mu$m. Dynamic viscosity, μ, is 1×10^{-3} Ns/m^2 for water at the room temperature is used. The result of the hydrodynamic resistance of device with respect to position of the valve is shown in Figure 2.13. According to this model, resistance of the microfluidic channel can be controllable from maximum value to nearly one-tenth of its maximum via actuating the valve. Besides the trapping function for cellomics applications, this characteristic can provide capability to use this device for different applications of microfluidics such as mixing, separation, or cell sorting applications.

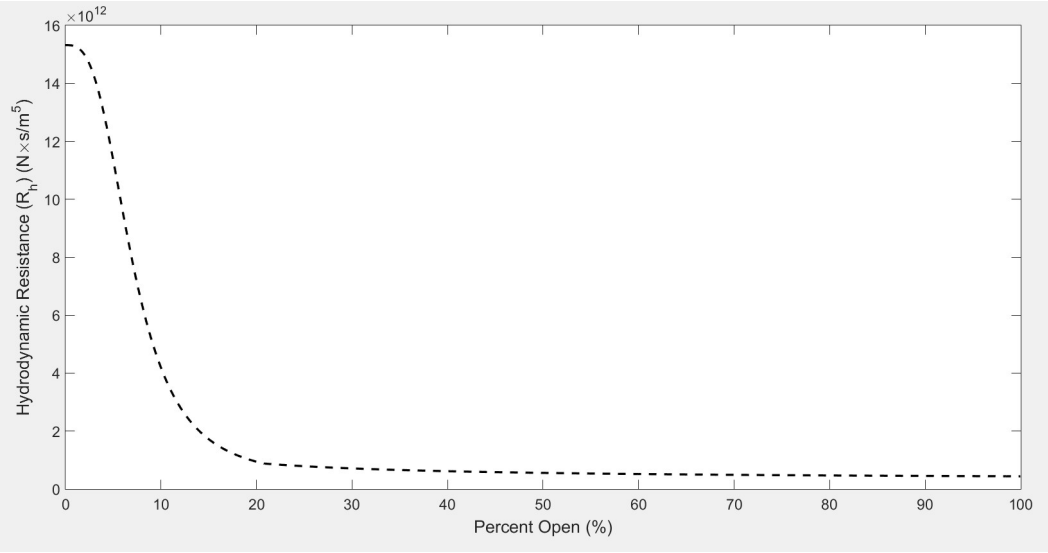

Figure 2.13. The result of the hydrodynamic resistance model of device with respect to position of the valve.

2.2.2. Flow Simulations of Microfluidic Device

In this section, flow simulations of microfluidic device via using COMSOL Multiphysics CAD tool is presented. Laminar flow module of COMSOL is used for observing

the velocity and the pressure drop in the channel for different positions of actuated valves. The geometry of the device with two valves at the inlet and the outlet and chamber is shown in Figure 2.14.

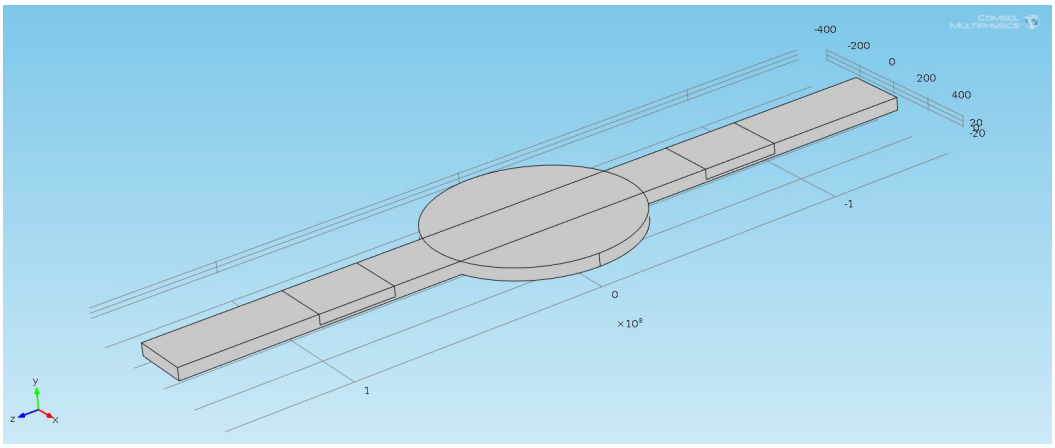

Figure 2.14. The geometry of the device with two valves at the inlet and the outlet and the chamber.

For modeling the valves, four variables are defined. Two of these determine the positions of the valves which take the opening percentage value as a parameter. The other two use these positions as a boundary and determine the fluid viscosity for the valve blocks. The opening percentage parameter is swept from 0 to 100 with the 10 percent step size. Water is chosen as a material and 0.1 m/s flow velocity is given from the inlet of the device. After solving this study in the laminar flow module with parametric sweep option, it gives the solutions of the velocity and the pressure drop distributions in the channel.

In Figure 2.15, the velocity distributions along the vertical cross section at the center of the device and the horizontal cross section at the center of the valve are shown for four different opening percentages of the valves.

When the microfluidic channel gets narrower due to the motion of the steel fingers, velocity of the water increases at this region under fixed flow rate applied. Maximum magnitudes of velocities in Figures 2.15a to 2.15h are 0.2045 m/s, 0.2023 m/s, 0.353 m/s, 0.3434 m/s, 0.8908 m/s, 0.8674 m/s, 0.155 m/s, and 0.6993 m/s, respec-

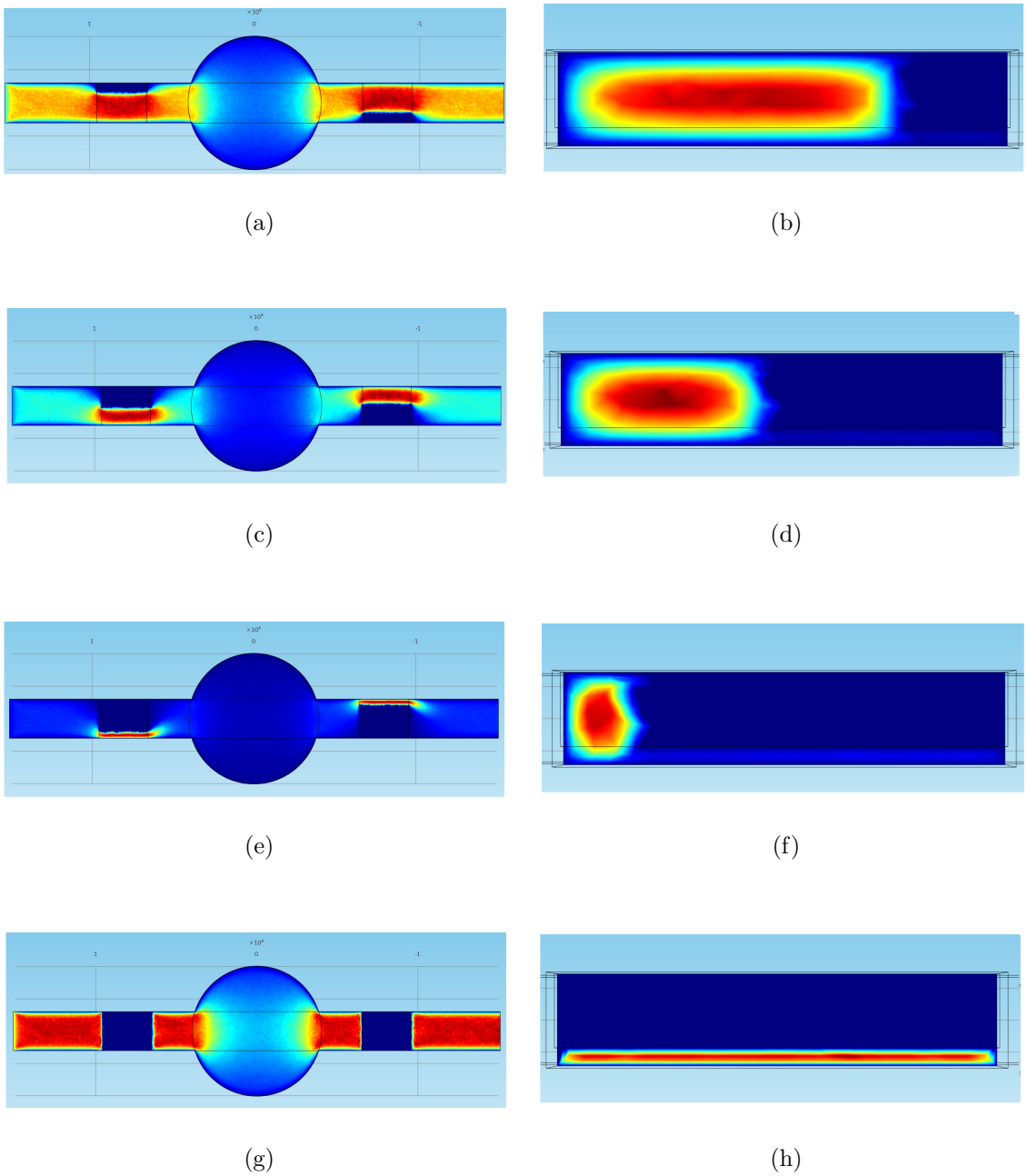

(a) (b)

(c) (d)

(e) (f)

(g) (h)

Figure 2.15. Velocity distributions along the vertical cross section at the center of the device and the horizontal cross section at the center of the valve, where the opening percentages are (a,b) 80%, (c,d) 50%, (e,f) 20%, and (g,h) 0%.

tively.

Figure 2.16 shows the results of pressure drop in channel for different opening percentages of valves. Maximum magnitudes of pressures in Figures 2.16a to 2.16e are 1392.6 Pa, 1528.8 Pa, 2018.1 Pa, 6057.4 Pa, and 34288 Pa, respectively. When the opening percentage of the channel decreases, the pressure drop concentrates on the valve region. Due to the fixed flow rate and increasing hydrodynamic resistance, maximum pressure in channel increases as expected.

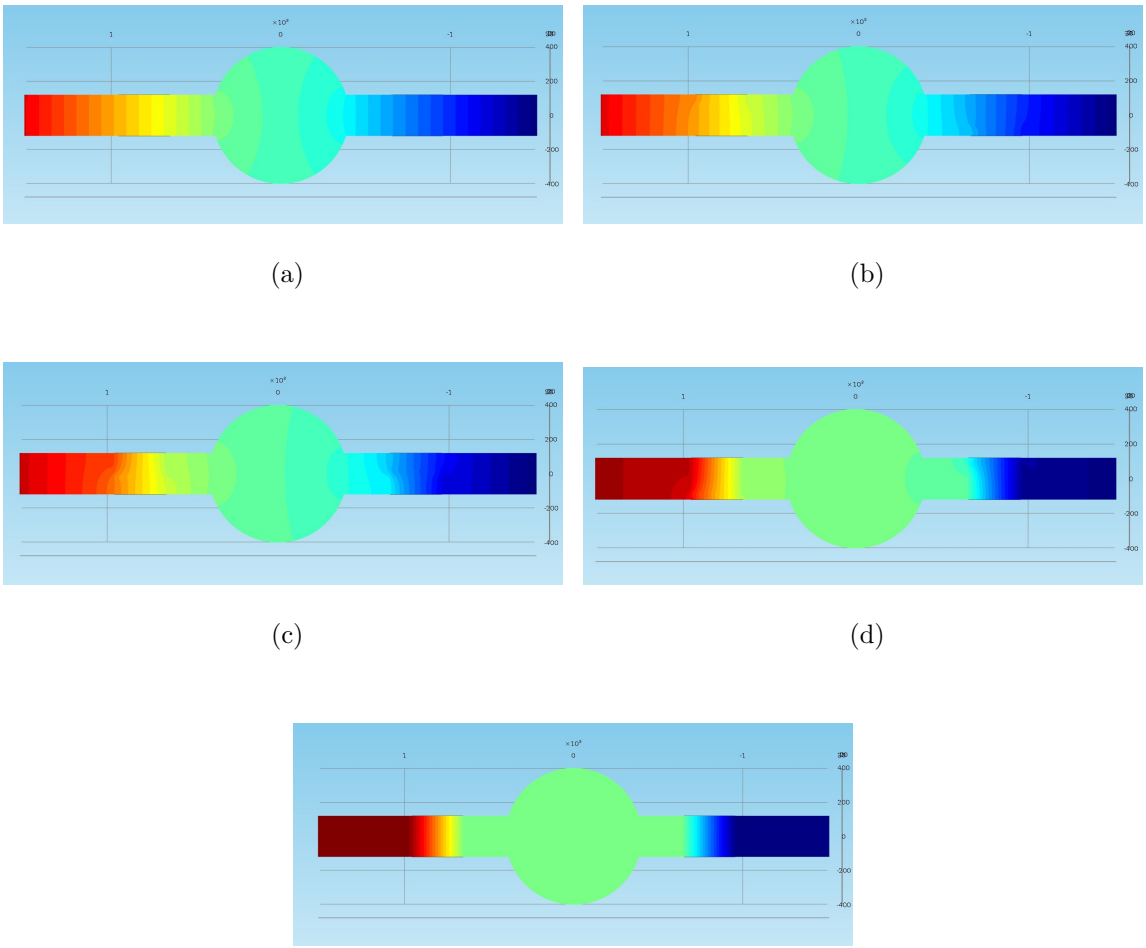

(a) (b)

(c) (d)

(e)

Figure 2.16. Results of pressure drop in channel, where the opening percentages of the valves are (a) 100%, (b) 80% , (c) 50%, (d) 20%, and (e) 0%.

To compare the results of the hydrodynamic resistance model of the channel which was presented in the previous section with the simulation results, microfluidic

channel with one valve is drawn with the dimensions that are used in the previous section. Simulations are done with parametric sweep of the opening percentage of the channel from 0 to 100 with the 10 percent step size. Then average pressure values of the inlet of the channel for all simulations are evaluated by using surface average tool of COMSOL under "Derived Values" menu. The flow rate of water is taken as $1.2 \times 10^{-9}\,\mathrm{m}^3/\mathrm{s}$. Using (2.6), hydrodynamic resistances of the device are calculated from simulation results. Figure 2.17 shows the results of hydrodynamic resistance derived from model and derived from the simulation.

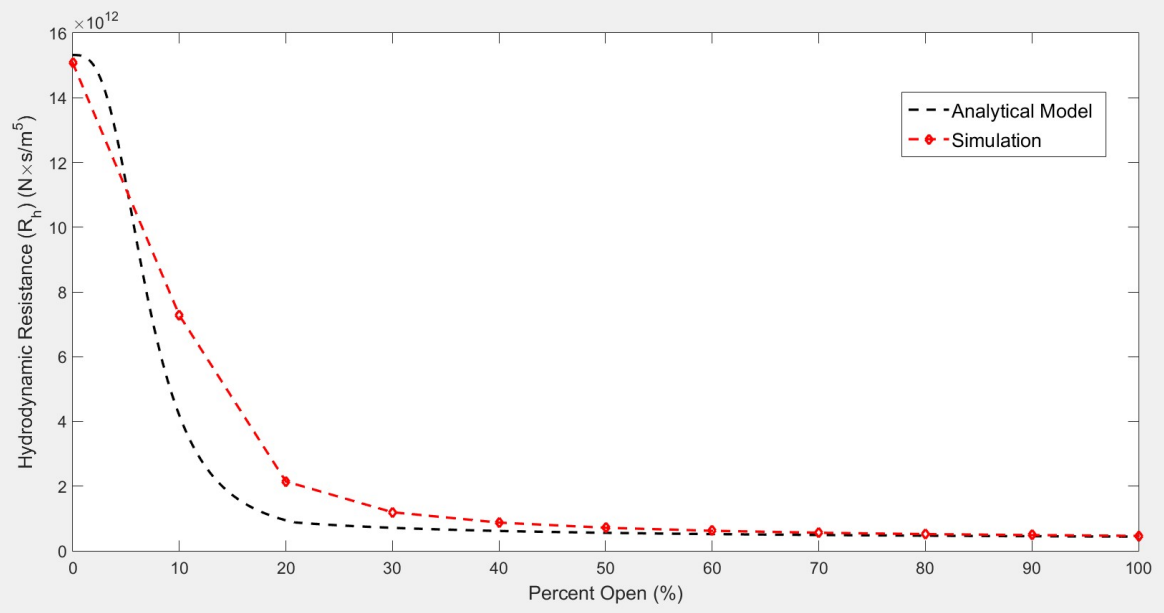

Figure 2.17. Results of hydrodynamic resistance derived from model and derived from the simulation.

3. STRUCTURE OF THE FABRICATED DEVICE

3.1. Fabrication

3.1.1. Photolithography of Steel Thin Film and Steel Mold

The first fabrication step of the microfluidic devices with steel displacement amplifiers is photolithography of the steel mold and the steel thin film. Steel mold with the dimensions of $100\,\text{mm} \times 100\,\text{mm} \times 0.5\,\text{mm}$, and the steel thin film (AISI 301) with the dimensions of $80\,\text{mm} \times 80\,\text{mm} \times 0.05\,\text{mm}$, is first cleaned and covered with photoresist (PR) using a spin coater. The steel thin film is strapped to a dummy silicon wafer with sticky tape for coating PR on a film homogeneously when it is spinning. After the spin coating is done, they are kept on a hot plate which is heated to $90\,^{\circ}\text{C}$ temperature for 2 minutes of soft baking process. Then, they are exposed to ultraviolet (UV) light under a mold and a steel device masks. Following this process, they are put into the PR developer for 45 seconds. After developing patterns on samples, they are cleaned with deionized (DI) water and they are again kept on hot plate at $110\,^{\circ}\text{C}$ temperature for 3 hours. This hard baking process is necessary for preserving PR during electrochemical etching process. In Figure 3.1, the samples after photolithography is shown.

3.1.2. Electrochemical Etching Process

Electrochemical etching is a process for etching a metal in electrolyte solution by using metals as electrodes and passing the electrical current on them. Positive terminal of the current source is connected to the metal to be etched, which is called the anode. Electrochemical etching process is illustrated in Figure 3.2.

Using three-dimensional (3D) printed parts, sealings, and water pipes, handmade electrochemical etching setup is built, as shown in Figure 3.3. Electrolyte solution which consists of DI water and sodium chloride ($4\,H_2O\ :\ 1\,NaCl$) is prepared. In

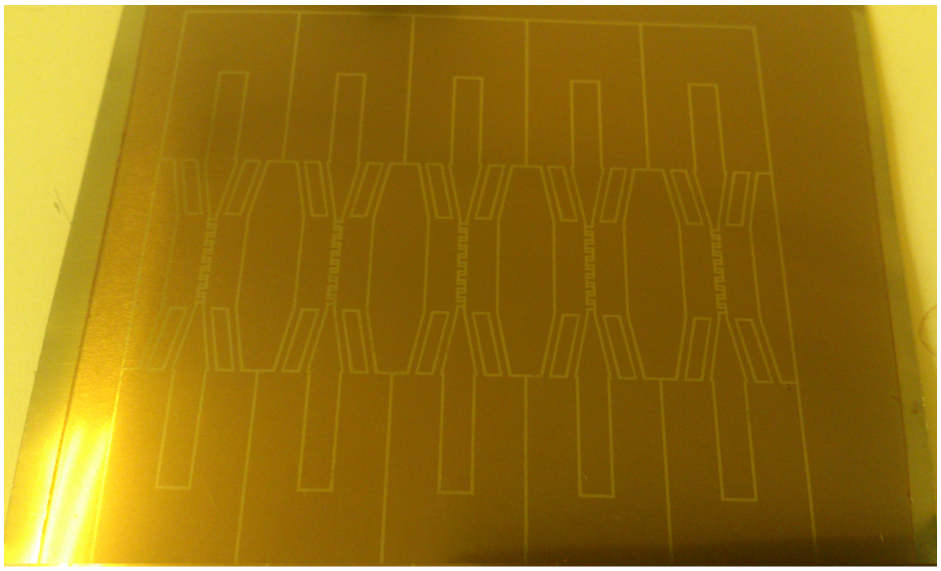

(a)

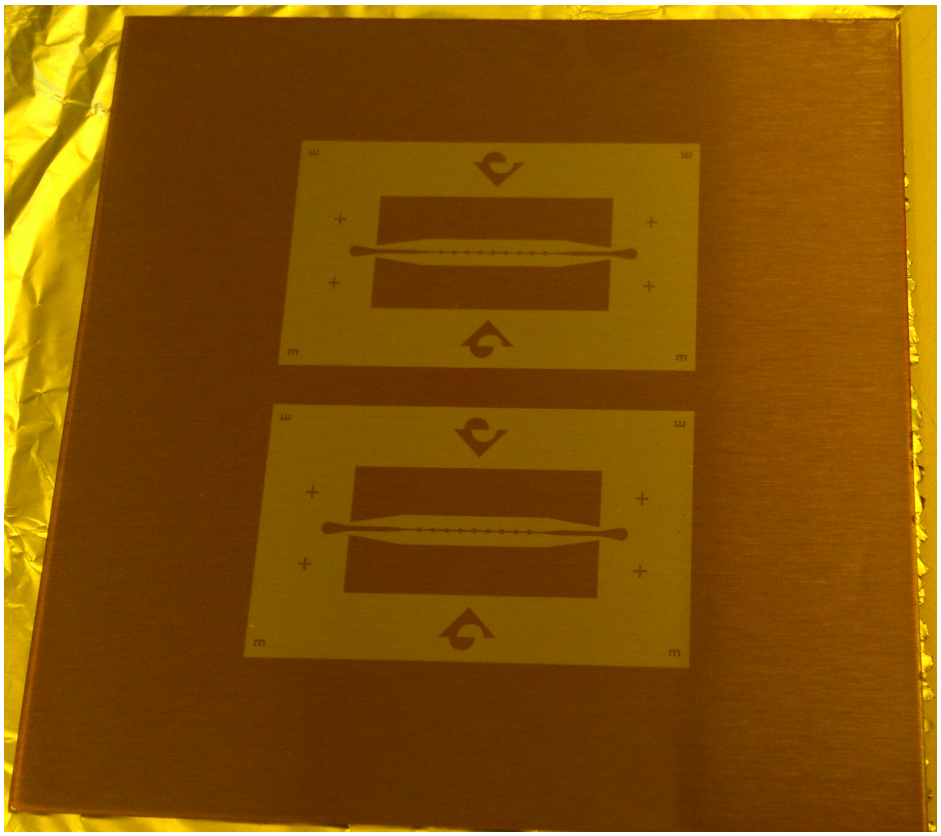

(b)

Figure 3.1. Sample of (a) steel displacement amplifiers, and (b) steel master plate after photolithography (old versions).

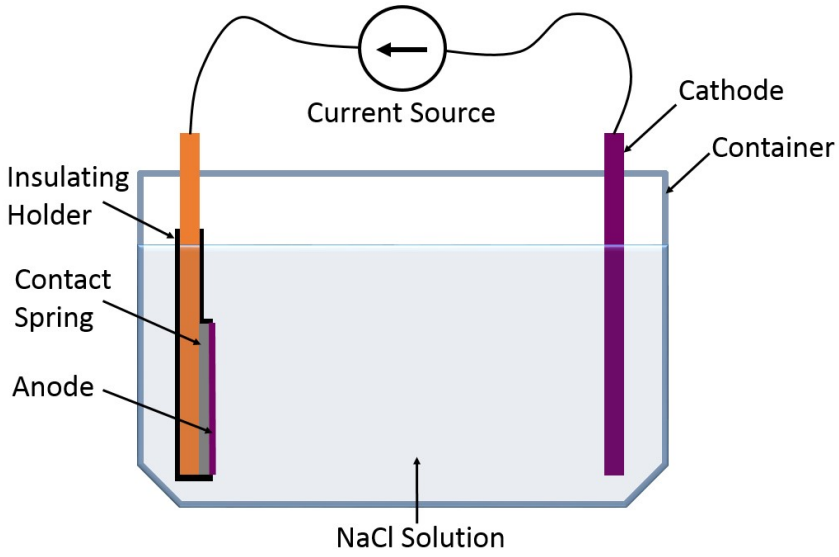

Figure 3.2. Illustration of the electrochemical etching process.

order to etch the steel, current density of $3\,\mathrm{A/cm^2}$ is applied during the electrochemical etching process [41].

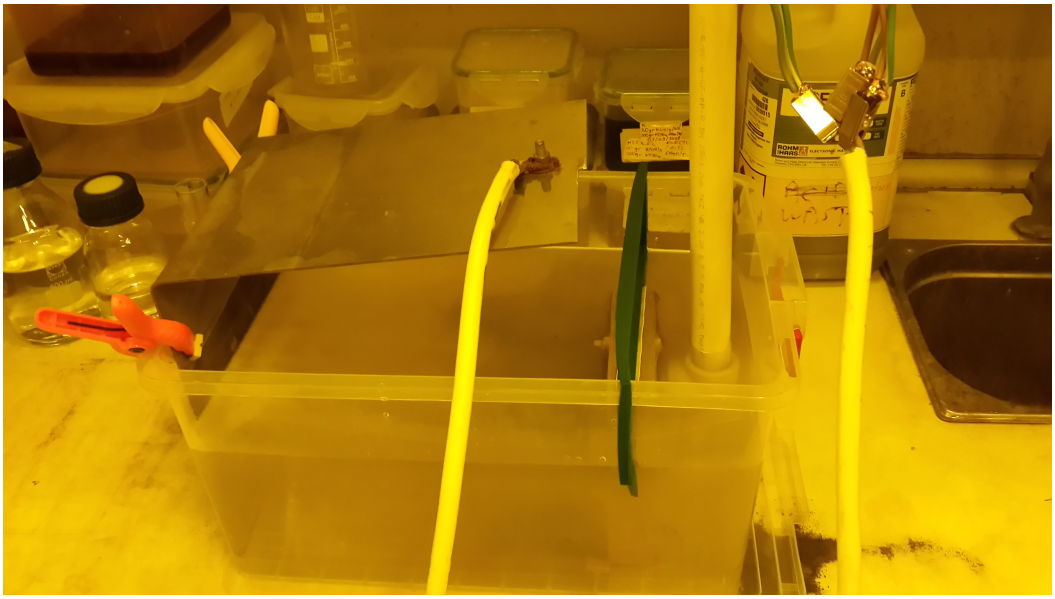

Figure 3.3. Handmade electrochemical etching setup.

Different heights of the channel and the suspension region are aimed to close the channel by fingers, whereas the steel beams that transfer and amplify the displacement can easily move in the suspended regions. For the etching of the steel mold, $50 - 55$ A current is applied for 40 seconds. After that process is paused, and the photoresist

on the microfluidic channel region is removed using acetone. Then, this process is continued for 40 seconds more to increase the height of the suspension regions. Figure 3.4 shows the steel mold after electrochemical etching. The height of the microfluidic channel is nearly 25μm, and the height of the suspension regions are nearly 50μm. In the regions where openings are large, the electrical field densities at the edges of the openings are higher, which increases the etch rates. In order to prevent this and obtain homogeneous etch rates on sample, a frame is added to design.

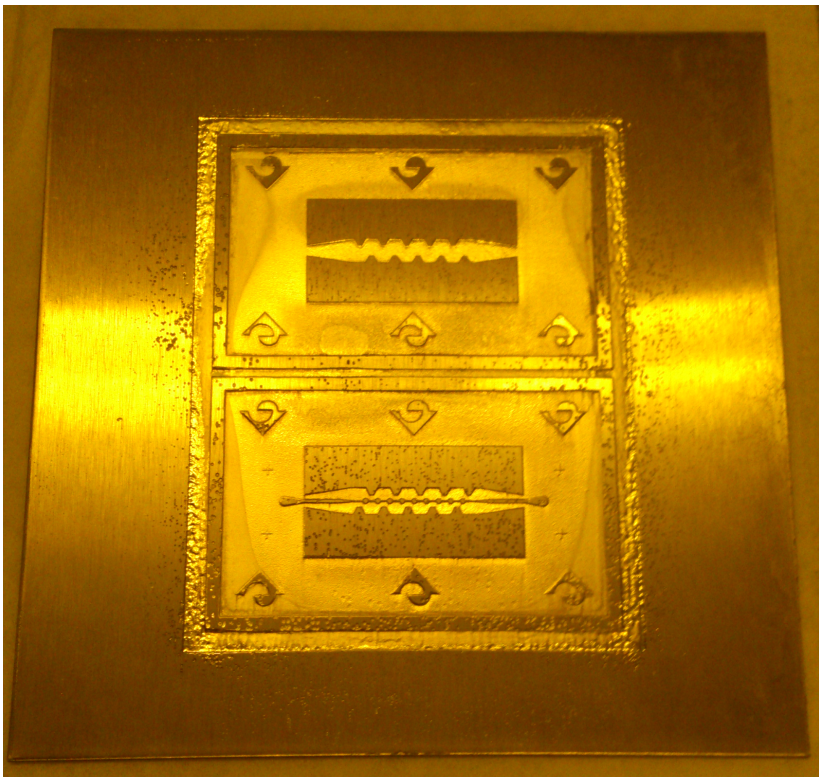

Figure 3.4. Steel mold after electrochemical etching.

For etching 50μm thick steel film, it is stretched on 0.5 mm thick steel substrate. In order to obtain homogeneous etch rates, inside the all openings more than 250μm width are covered with PR and 250μm wide frames are left open. Thus, etching process is mass transport limited, and more controllable. 9 A current is applied for 2 minutes. Figure 3.5 shows the steel thin film after electrochemical etching. There are 4 steel devices that can be fabricated at the same time. The electrical field at the outer openings is more dense then the openings around fingers and the beams. For this reason, the outer frame is fully etched but there are some residual steel parts

between the fingers, and the beams.

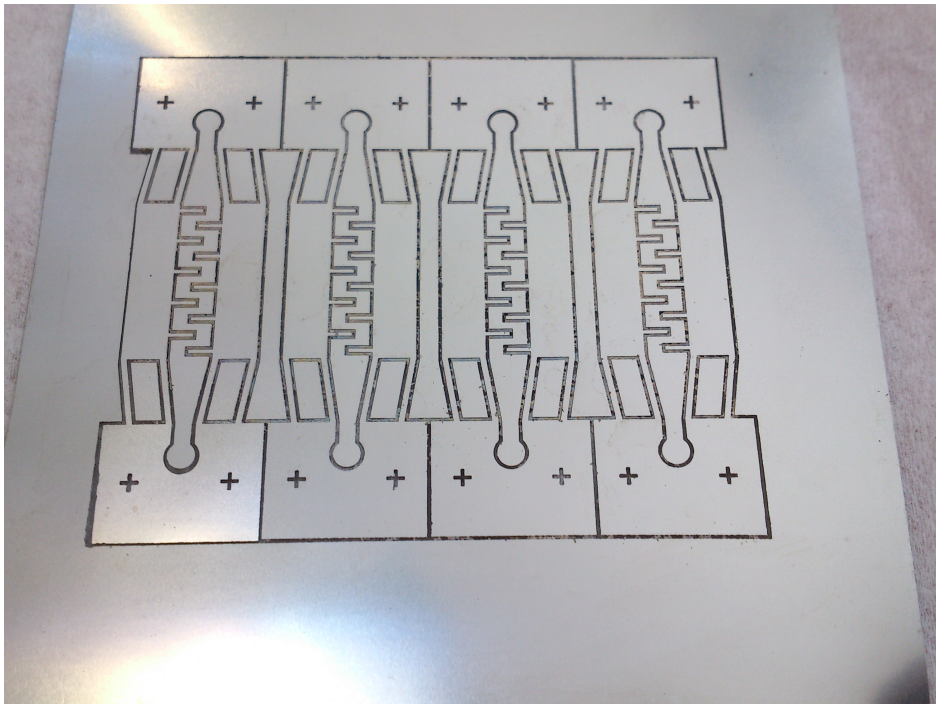

Figure 3.5. Steel thin film after electrochemical etching.

3.1.3. Chemical (Wet) Etching Process

In order to remove the residual steel parts after electrochemical etching of steel thin film and smoothen the edges of the device, thin film is wet etched in steel etchant solution. It consists of nitric acid, hydrochloric acid and DI water ($1\,HNO_3$: $3\,HCl$: $10\,H_2O$) [42]. Due to unknown thickness of oxide on the device, the duration of the process cannot be determined. For this reason, this process should be kept under observation. When the steel devices release their residual parts, this process should be terminated. It takes $1-2$ hours with respect to thickness of the oxide. Figure 3.6 shows devices after wet etching. The thickness of the device can vary between 35μm to 40μm with respect to time of the process.

3.1.4. Hot Embossing and Bonding of the PMMA Plates

There are three steps in this process, which are hot embossing of two PMMA plates ($30\,\text{mm} \times 50\,\text{mm} \times 1\,\text{mm}$) using steel mold, hot embossing of PMMA plate with

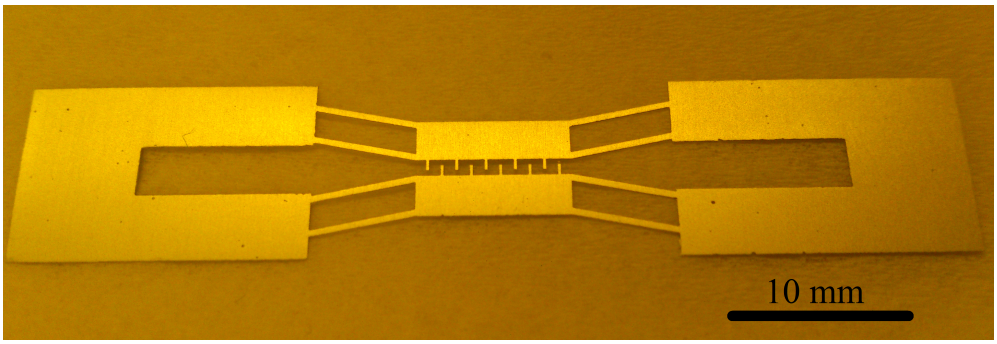

(a)

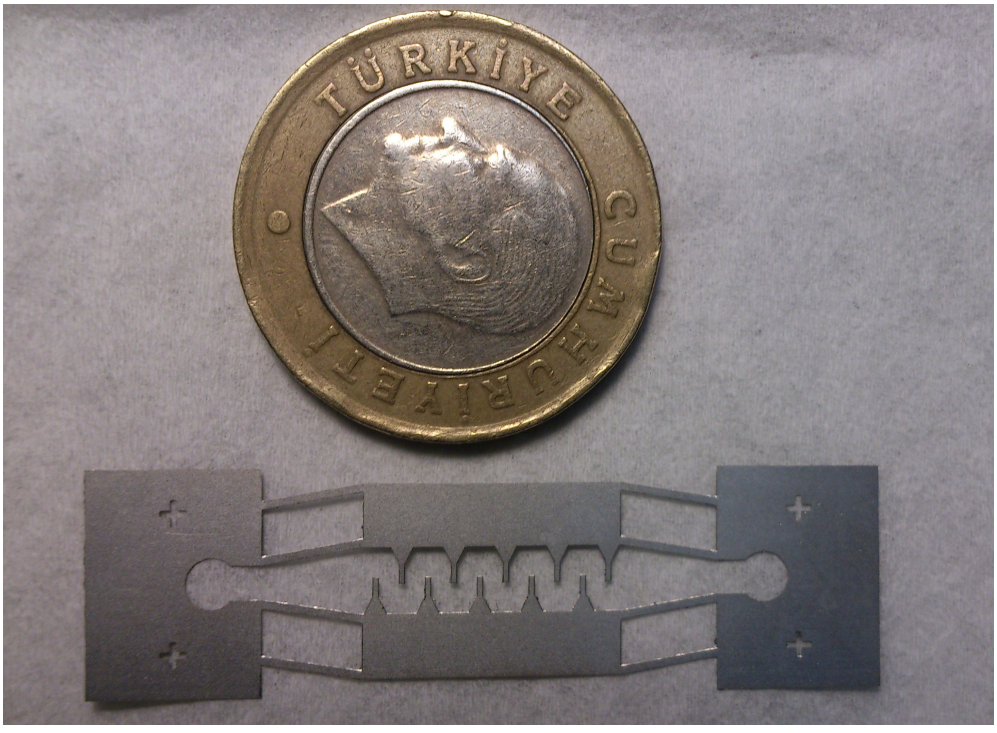

(b)

Figure 3.6. Steel displacement amplifiers after wet etching, where the devices are (a) normally-on, and (b) normally-off.

the microfluidic channel patterned on it using steel displacement amplifier with finger shaped structures, and bonding of PMMA plates. These steps are illustrated in Figure 3.7. The glass transition temperature of the PMMA is around 105°C. Hot embossing temperature should be above the glass transition temperature, and bonding temperature should be below it to protect the embossed structures.

In the first step, hot embossing of PMMA plates with steel master plate to form channel and the suspension regions is done. The top and the bottom plates of the press machine is heated to 120°C temperature. 1 mm thick PMMA plates are embossed with steel master plate under 1250 pounds of load for 10 minutes. Then, heaters are turned off and plates are cooled to 60°C temperature under load before they are taken out. PMMA plates after hot embossing is shown in Figure 3.8.

In the second step, hot embossing of the PMMA plate, that microfluidic channel and suspension pools are formed on it, with steel displacement amplifier is done, to embed anchor regions and fingers on it. In order to preserve microfluidic channel and suspension pools, only one plate of press machine which is at side of the steel device is heated to 110°C temperature. Plate is embossed with steel device under 500 pounds of load for 10 minutes. Then, heaters are turned off and plates are cooled to 60°C temperature under load before they are taken out.

In the third step, PMMA plate with that device is embedded on it, and the other PMMA cover plate with that suspension pools are formed on it, are bonded. These two plates are cleaned first. Then they are put in 2-propanol for 10 minutes in order to active their surfaces. After that, they are aligned via using alignment markers. The top and the bottom plates of the press machine is heated to 80°C temperature. Thermo-compression bonding of device is done under 750 pounds of load. Figure 3.9 shows the device after bonding.

After the bonding process, buckling and deformations on steel device between two PMMA plates are observed. Steel device is not actuated as it was expected under the force applied from the two sides of plates. To comprehend the problem, suspension

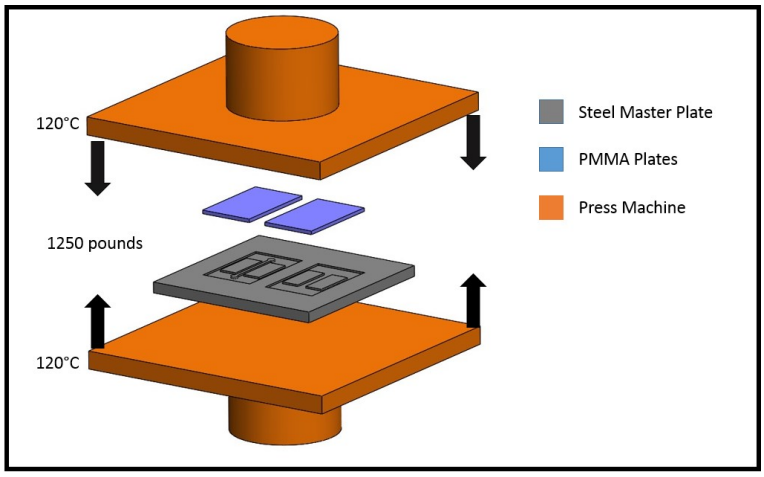

(a)

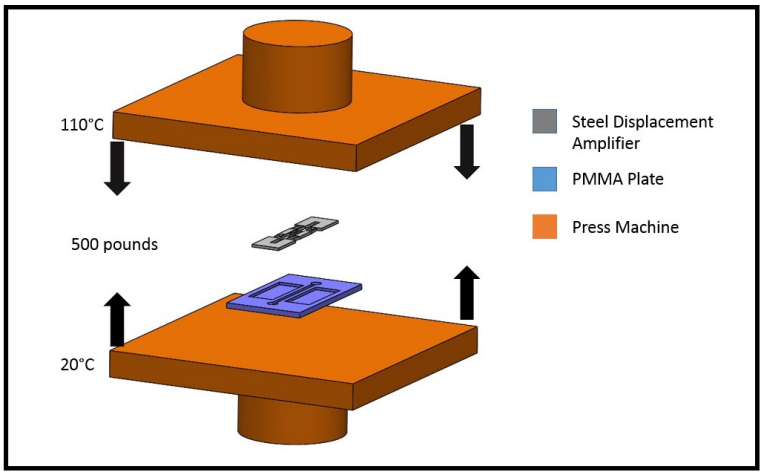

(b)

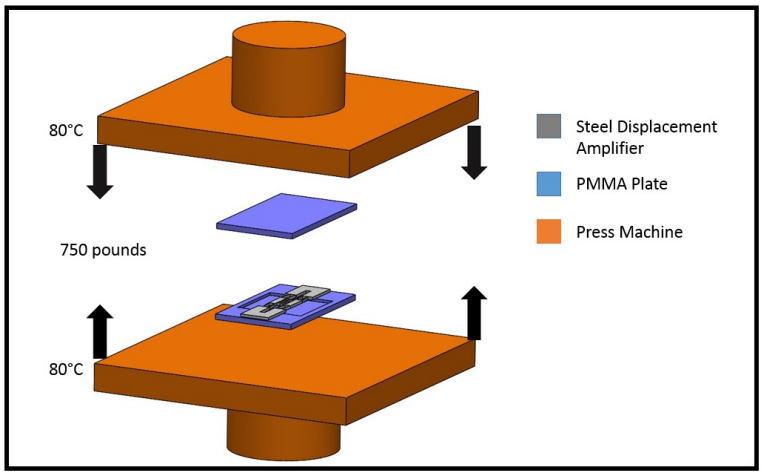

(c)

Figure 3.7. Illustration of hot embossing and bonding steps of PMMA.

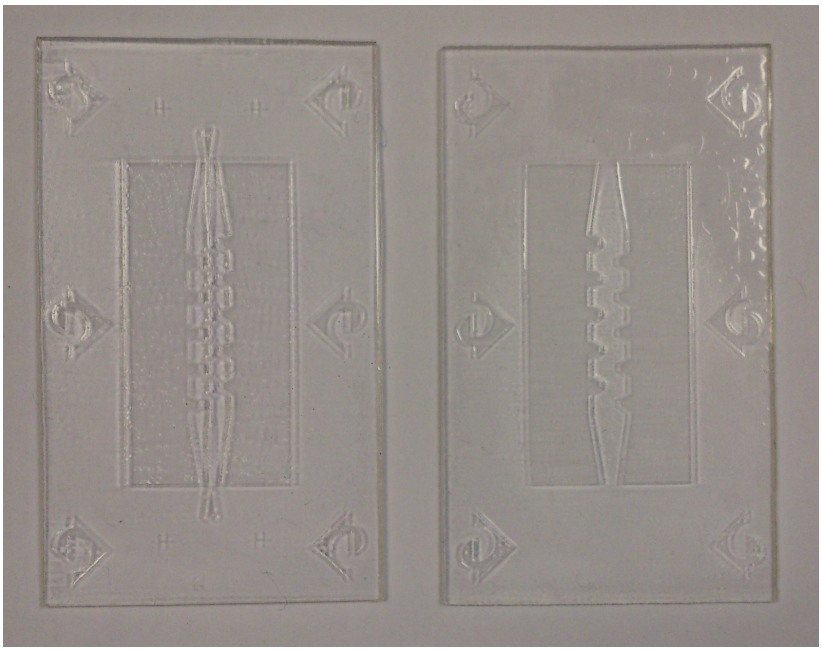

Figure 3.8. PMMA plates after hot embossing.

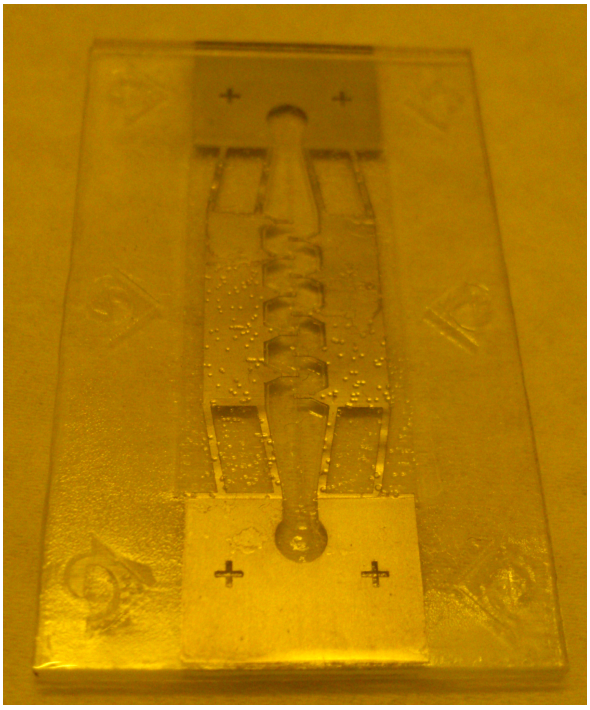

Figure 3.9. The device after bonding.

regions of the PMMA plates are cut via using laser. After second step is repeated with these plates, buckling is clearly observed like shown in Figure 3.10. The coefficient of thermal expansion (CTE) of PMMA ($50 \times 10^{-6}\,K^{-1}$– $100 \times 10^{-6}\,K^{-1}$) is higher than CTE of Stainless Steel ($10 \times 10^{-6}\,K^{-1}$– $17 \times 10^{-6}\,K^{-1}$), which means CTE difference causes this problem, which will be discussed in next chapter.

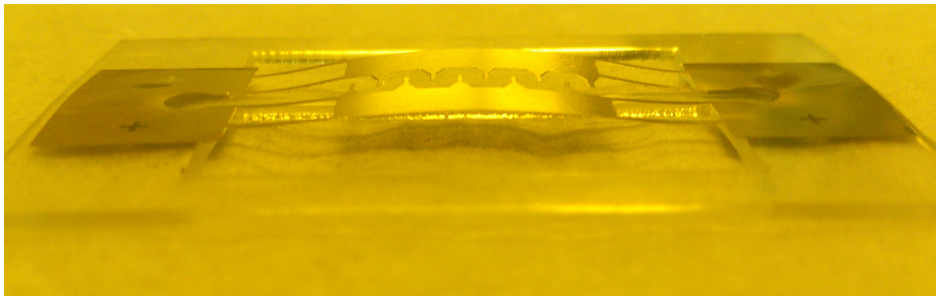

Figure 3.10. Buckling of steel device after hot embossing.

3.1.5. Laser Micromachining Process

After unexpected results obtained from studies with PMMA, studies are focused on polyethylene naphthalate (PEN) which has CTE of $17 \times 10^{-6}\,K^{-1}$ that is very close to CTE of stainless steel. 125μm thick DuPont Teijin Q65FA heat stabilized PEN film is used for these studies. In consideration of the lack of time, laser micromachining technique which is a faster way to fabricate prototypes of microfluidic devices [43, 44] is used to engrave microfluidic channel and cut openings for suspension region. VersaLASER VL-200 is used as engraving and cutting device. Figure 3.11 shows the PEN film after laser micromachining.

Microfluidic channels are engraved on the PEN film with the system speed of 10% and the system power of 1%. The measured width of the engraved channel is about 300μm and the measured height of the engraved channel is around 30μm−35μm. The system speed of 5% and the system power of 1% is adjusted to cut the 125μm thick PEN film.

Because the device is actuated by mechanical force and the PEN film is very thin that it cannot be actuated without buckling, the substrate and the cover PMMA

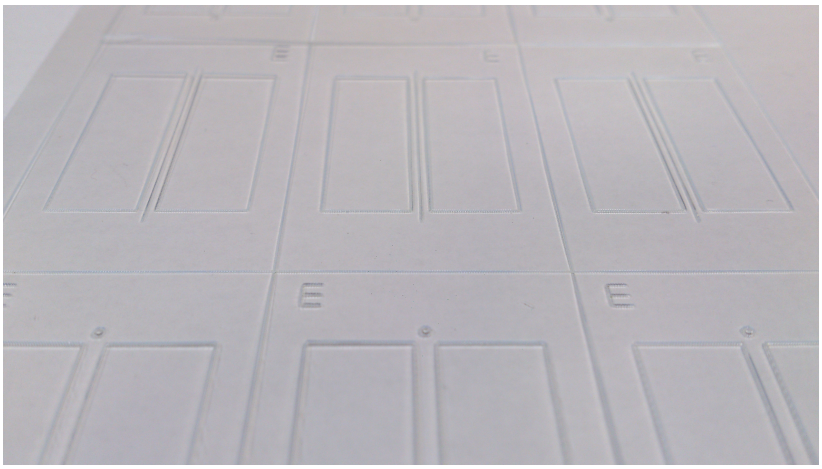

Figure 3.11. PEN film after laser micromachining.

plates are also cut by using laser, shown in Figure 3.12. The system speed of 3% and the system power of 90% is adjusted to cut the 1 mm thick PMMA plate.

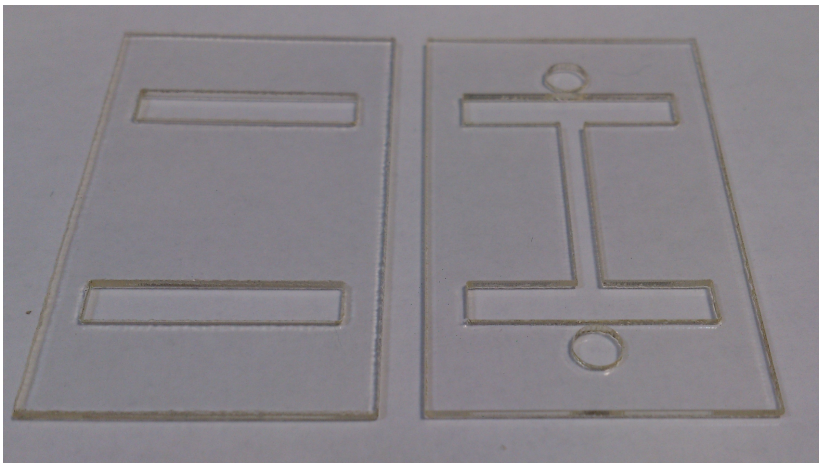

Figure 3.12. PMMA plates, cut by using laser.

3.1.6. Hot Embossing and Bonding of the PEN films

This process is very similar to hot embossing and bonding of the PMMA plates, except there are two steps for this process. The first step is skipped by using laser micromachining mentioned in the previous section. The glass transition temperature of the PEN is around 120°C temperature and it has higher Young's modulus than PMMA which means the temperatures and the pressures of these two steps should be higher than steps of PMMA hot embossing and bonding.

Hot embossing of PEN film, that microfluidic channel is engraved and suspension regions are cut by laser, with steel displacement amplifier to embed anchor regions and fingers on it is done. The top and the bottom plates of the press machine is heated to 140°C temperature. Plate is embossed with steel device under 2500 pounds of load for 10 minutes. Then, heaters are turned off and plates are cooled to 60°C temperature under load before it is taken out. Figure 3.13 shows the PEN film after steel device is embedded. There is no buckling or deformation is observed unlike shown in Figure 3.10.

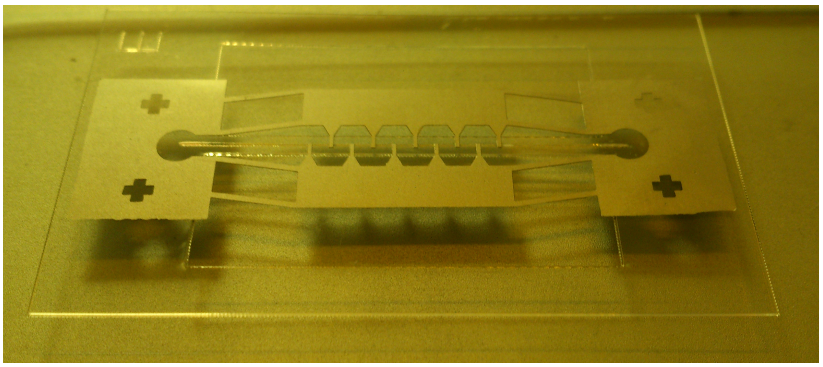

Figure 3.13. PEN film after steel device is embedded, via hot embossing.

Bonding of PEN film that device is embedded on it and the other PEN cover plate that suspension pools and the input and the output ports are cut is done. These two plates are cleaned first with 2-propanol and DI water. Then they are put in chloroform stabilized with ethanol ($1\,CHCl_3 \;:\; 1\,C_2H_6O$) for 3 minutes in order to active their surfaces. One sides of these films were pretreated in order to improve bonding. After surface activating they are gathered together such that these pretreated surfaces face each other and aligned. The top and the bottom plates of the press machine is heated to 125°C temperature. Thermo-compression bonding of device is done under 1500 pounds of load. Figure 3.14 shows the device after bonding.

After fabricating the microfluidic device with steel displacement amplifier, it should be attached to substrates in order to prevent buckling or deformation. The device is pasted to 1 mm thick PMMA substrate and cover plates using epoxy. Figure 3.15 shows the device after fabrication is done.

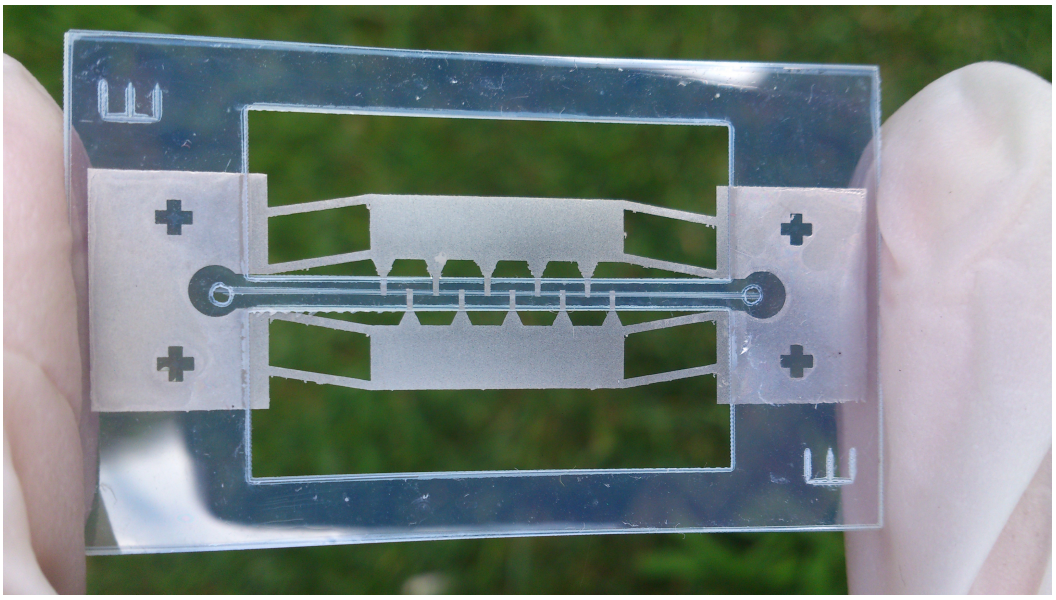

Figure 3.14. Device after bonding.

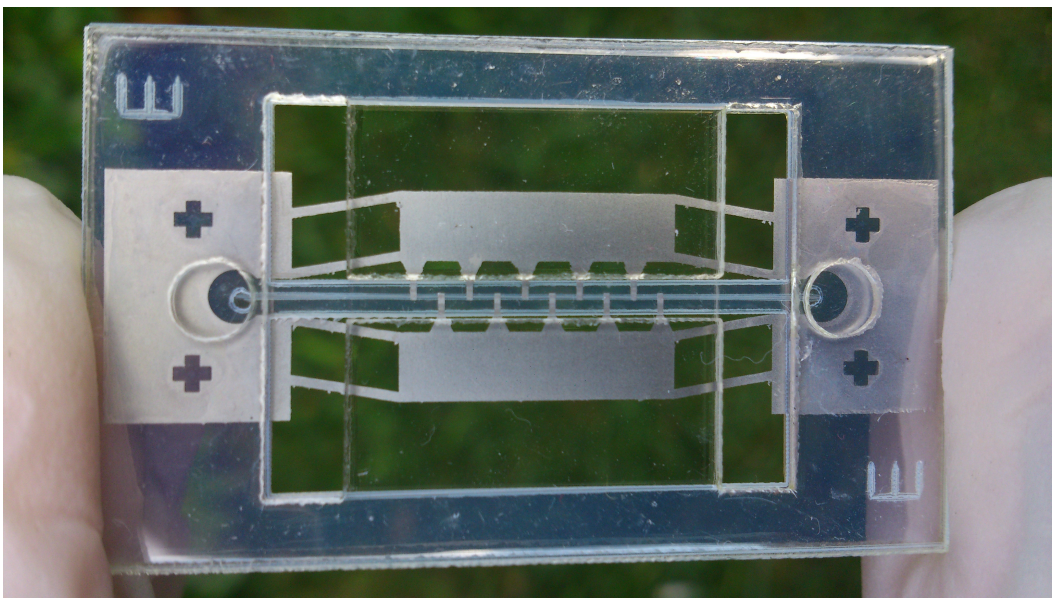

Figure 3.15. Device after fabrication.

4. MEASUREMENTS AND CHARACTERIZATION OF THE DEVICE

4.1. Dimensional Measurements on Fabricated Steel Devices

In this section, dimensional measurements of 4 steel devices that fabricated in the same batch are done via using a measurement microscope (Nikon MM400 L). In order to characterize the electrochemical etching process, more than 400 measurements are taken from the different parts of these 4 devices, and measurement data is compared to the original dimensions that are used to draw a mask. Also measurements taken from each sample are compared between each other to evaluate the reproducibility of the device, and the consistency of the process.

For electrochemical etching process, undercut effect should be considered because this process is like an isotropic etching which means etching process is happened in all directions equally. In Figure 4.1, undercut effect is illustrated. For this reason, undercut effect should be considered to get accurate results from electrochemical etching process.

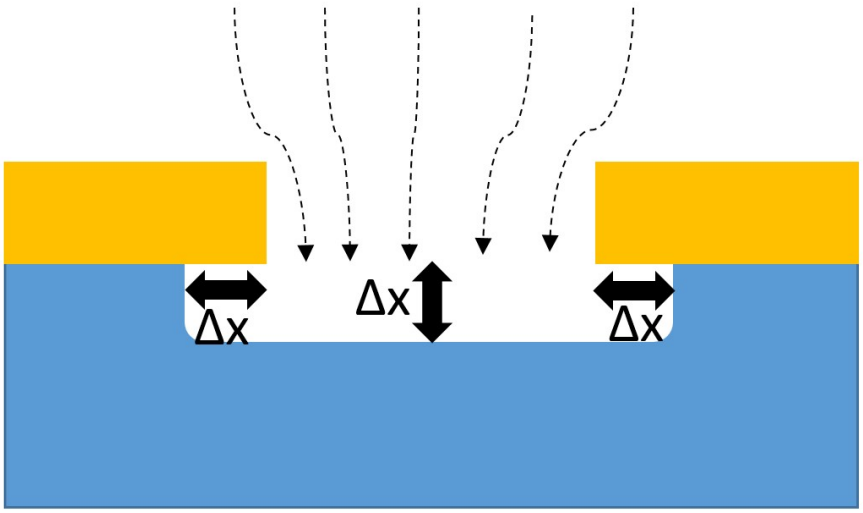

Figure 4.1. Illustration of the undercut effect.

To characterize the electrochemical etching process, 112 dimensions are mea-

sured from each 4 steel displacement amplifiers, fabricated in a same batch. The same dimensions are grouped and average of these measurements are taken for each group of each sample individually. Then average of each group for 4 samples are also taken to compare with the original dimensions from the mask drawing. The undercut effect causes increase, decrease or no change in dimensions with respect to convexity or concavity of the shapes, which is also considered in this comparison. Figure 4.2 shows the comparison results of 13 groups of dimensions for both considering or not considering undercut effect.

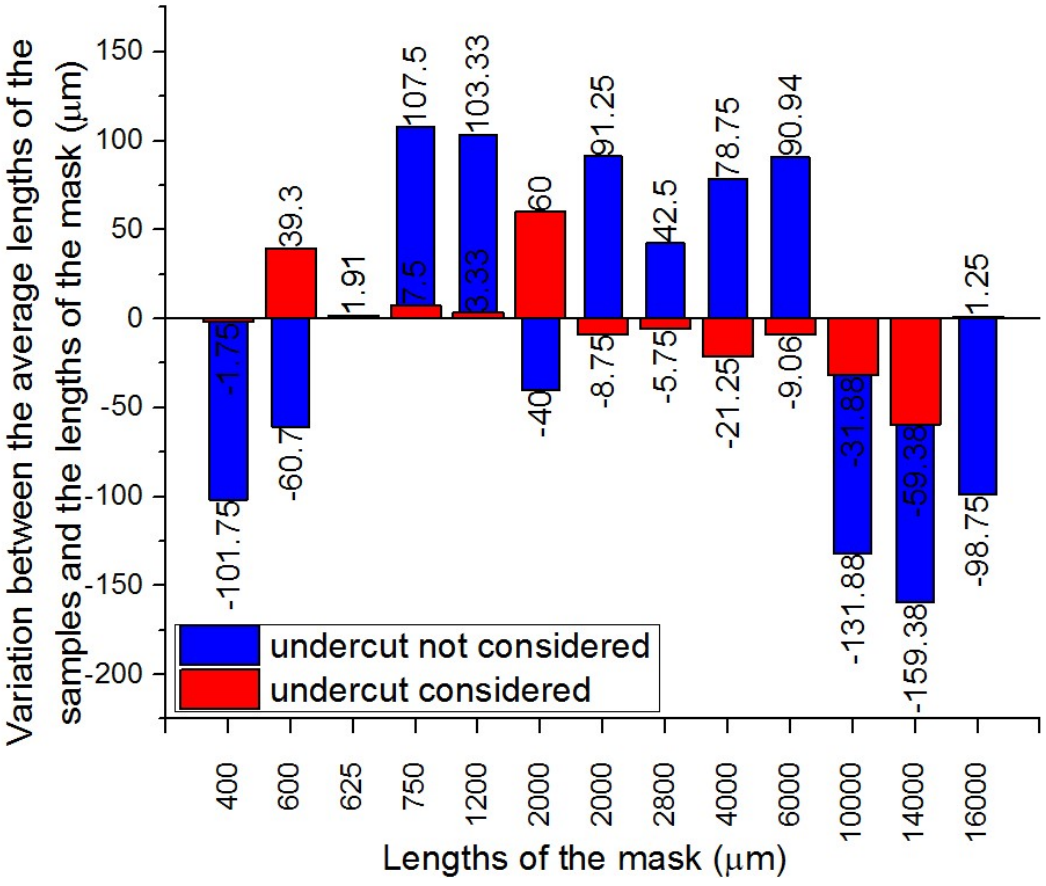

Figure 4.2. Comparison results of 13 groups of dimensions, measured from 4 samples.

These results show that undercut effect is effective for electrochemical etching process as expected. There is also side effect which is nonhomogeneous distribution of the electrical field during etching process can be deduced from these results. The outer openings of the mask has more etch rate than the inner openings around finger shapes, where electrical field density should be less than the outer frames due to more

openings per area. Also because of the high electrical field density of the sharp edges, etch rate of these regions are more than the other regions. According to these results, it can be said that 50μm thick metal devices with 100μm of minimum feature size can easily be fabricated via using this method, which is quite sufficient for the work done in this thesis. These results also show that the process can be more controllable when these effects are taken into consideration. To discuss these side effects, collecting more data from less complex shaped devices fabricated via using electrochemical etching can be useful. It can be predicted from these results that, minimum feature size of 20μm can be reached when the undercut effect and the electrical field density distribution is considered as side effects.

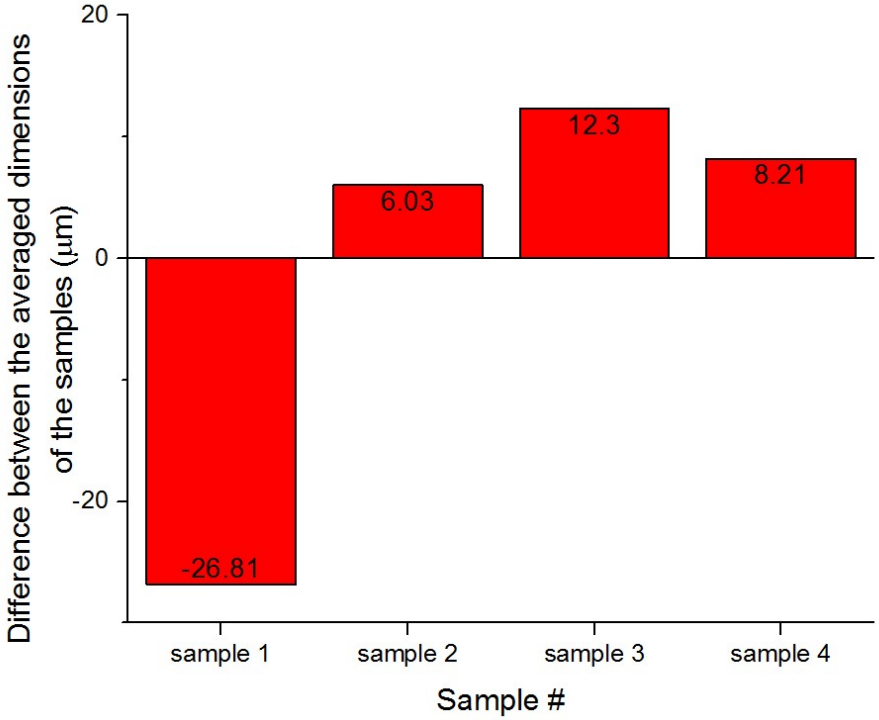

Figure 4.3. Variation between average dimensions of the samples.

Figure 4.3 shows the variation between average dimensions of these 4 samples. It shows that the process is suitable for batch fabrication. The standard deviation is also calculated as 15.63μm.

4.2. Force vs. Displacement Measurements of Steel Displacement Amplifier

In this section, results of displacement measurements on steel displacement amplifier under different loads are presented. The applied force is measured by a load cell. Figure 4.4 shows the measurement setup.

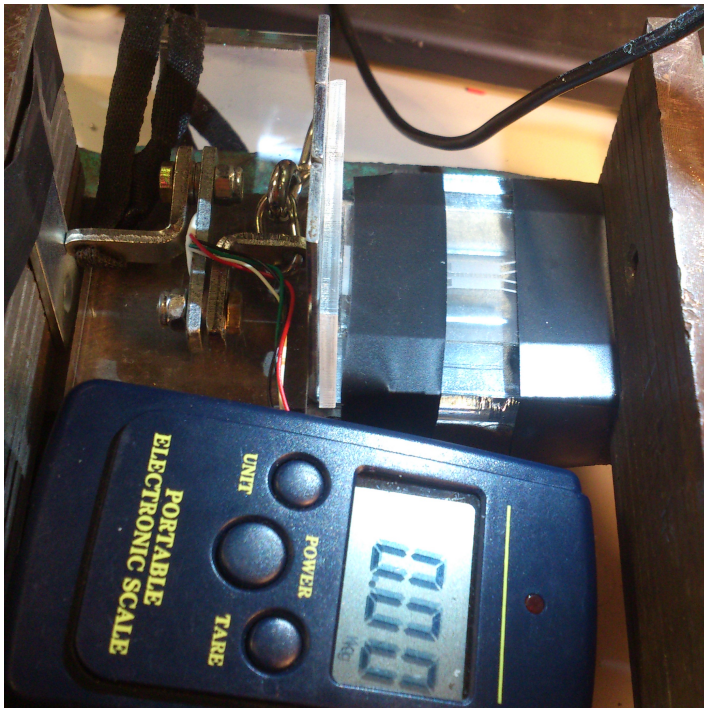

Figure 4.4. Measurement setup of the steel displacement amplifier.

Clamping device is used to apply force and to prevent the buckling or the motion in z-direction, device is supported with steel parts and adhesive tapes. Steel device is bonded to two PMMA plates, which are hot embossed to form suspension regions, with using epoxy. Figure 4.5 shows the measurements of the normally on device under microscope.

Figure 4.6 shows the displacements of steel fingers under different loads. Results show that device can be actuated with the expected ranges of the applied force. The measured displacement values are lower than the simulation or the analytical results. Due to unknown properties of the materials that are used to realize this device, sensible comparison of the results is not possible. Also using epoxy to bond the steel device

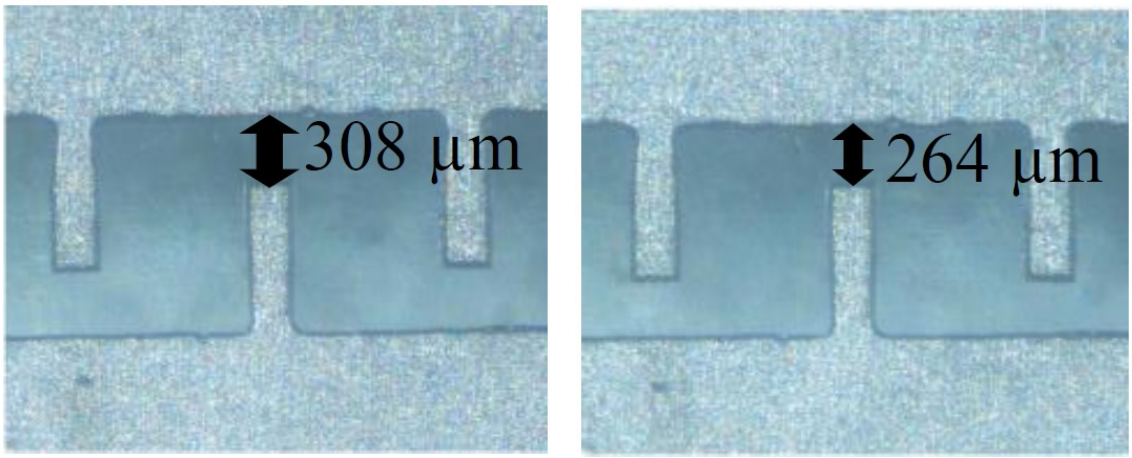

(a) (b)

Figure 4.5. Measurements of the normally on device under microscope.

to the PMMA plates can manipulate these results. But it can be said that the device can operate linearly with the expected applied force range.

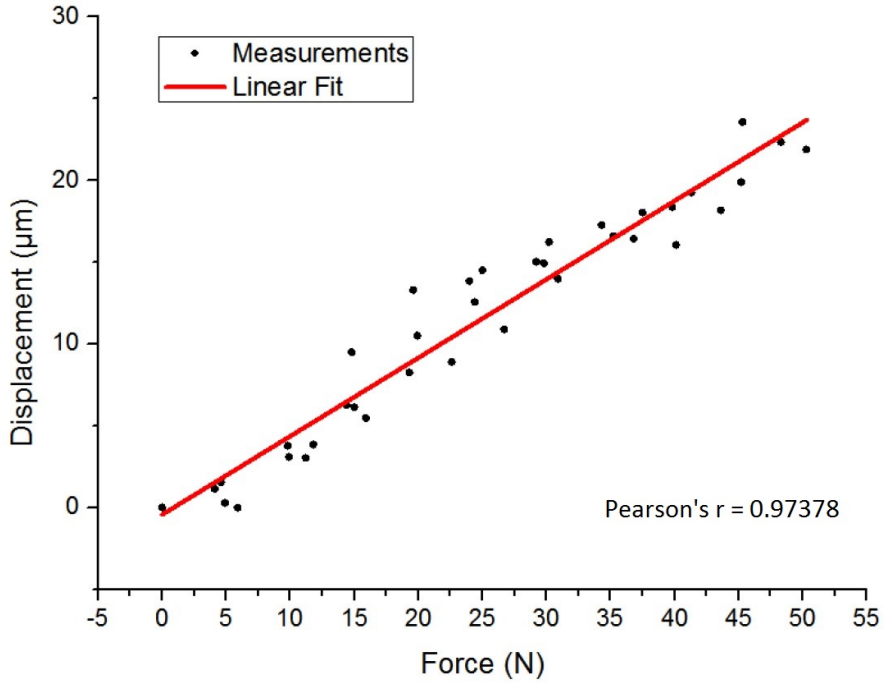

Figure 4.6. Displacements of steel fingers under different loads.

4.3. Coefficient of Thermal Expansion Differences of the Stainless Steel and the PMMA

As mentioned in the previous chapter, mismatch between CTE's of the steel and the PMMA causes integration problem during the hot embossing process of fabrication. In this section, the measurement results of the CTE difference between stainless steel (AISI 301) and the PMMA is presented. The change in linear dimension can be estimated by using following formula

$$\frac{\Delta L}{L_0} = \alpha_L \times \Delta T, \tag{4.1}$$

where ΔL, L_0, α_L and ΔT denote the change in length, initial length, linear expansion coefficient of material, and the change in temperature, respectively.

The hot embossing process of steel device and PMMA plate happens at 110°C temperature, and the CTE of PMMA (50×10^{-6} K^{-1}–100×10^{-6} $K^{-}1$) is higher than CTE of Stainless Steel (10×10^{-6} K^{-1}–17×10^{-6} $K^{-}1$). When samples are cooled down to the room temperature, PMMA shrinks more than the steel which generates the stress on steel device. This stress causes the buckling or deformation on steel as shown in Figure 3.10.

To estimate the CTE difference, hot embossing of steel device with PMMA plate is done at 120°C temperature and the steel device is taken off from PMMA plate at that temperature. After samples are cooled down to room temperature, dimensional measurements on steel device and the PMMA plate is done under measurement microscope. Figure 4.7 shows the results of these measurements.

Initial lengths of the steel and the PMMA is same at 120°C temperature because PMMA is formed by using steel at this temperature. With using (4.1), CTE difference

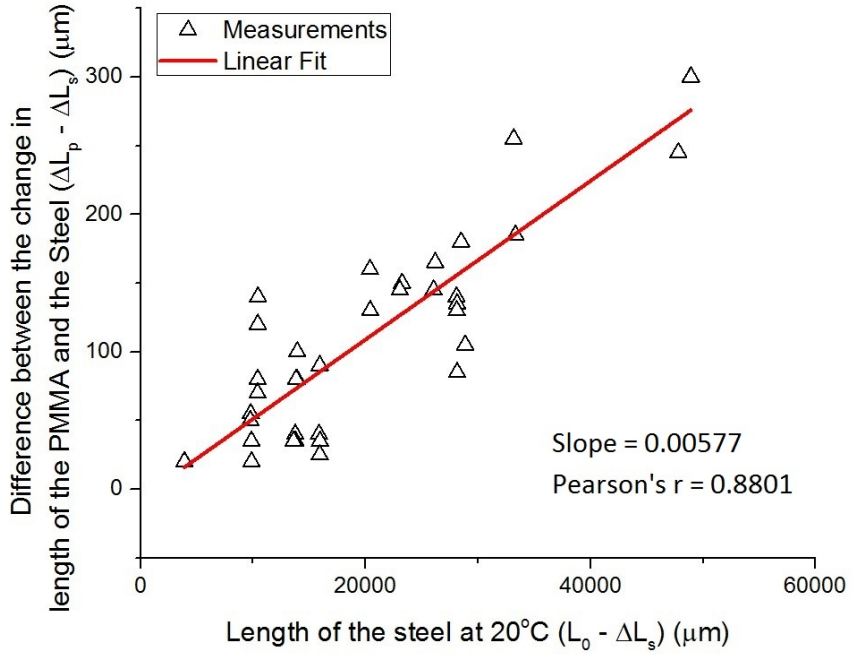

Figure 4.7. Measurements of the difference between the dimensions of the PMMA plate and the steel device, due to CTE mismatch.

of steel and the PMMA can be calculated as

$$(\alpha_p - \alpha_s) = \frac{(\Delta L_p - \Delta L_s)}{L_0} \times \Delta T, \tag{4.2}$$

where α_p, α_s, ΔL_p and ΔL_s denote the linear thermal expansion coefficient of PMMA, the linear thermal expansion coefficient of steel, the change in the length of steel, and the change in the length of PMMA, respectively.

Slope of the linear fit of the data gives $(\Delta L_p - \Delta L_s)/(L_0 - \Delta L_s)$, where the temperature difference is taken as $\Delta T = 100°\text{C}$. ΔL_s value at the denominator can be negligible for these measurements because the measured values are much bigger than the ΔL_s. It is assumed that slope gives $(\Delta L_p - \Delta L_s)/L_0$. Using (4.2), the linear thermal expansion coefficient difference between the PMMA and the steel that are used

to realize these devices can be found as $57.7 \times 10^{-6}\,\mathrm{K}^{-1}$ which is quite acceptable in the expected ranges given in the literature.

Using this result to redesign the steel master plate, and the steel displacement amplifier can solve this problem. On the other hand, there is no datasheet found for these materials used in this work. Additionally, CTE changes with the temperature, thus, it is not a good solution for reproducibility of the device and the sustainable fabrication. Hence, final devices are fabricated using PEN substrates which have almost the same CTE as the steel thin films.

5. CONCLUSION AND FUTURE WORK

In this thesis, microfluidic devices with steel displacement amplifiers are designed, analyzed and fabricated. After fabrication, devices are redesigned and refabricated several times in order to solve some problems that are encountered within this period. In this chapter, studies that are presented in previous chapters are summarized and the final results are discussed. In the light of this information, future work that can be done is also evaluated.

As mentioned in the first chapter, the main goal of this study is to fabricate microfluidic devices with simple trapping mechanism to use them for cell culturing and analysis applications. In addition to this, based on the ease of usage of the device, and using cost-efficient and rapid fabrication methods, the novel idea is presented. Using compliant mechanisms like displacement amplification mechanism in microfluidic devices can provide practical solutions for many applications of microfluidics.

In Chapter 2, description of the device is presented with the CAD tool simulations and models. The principle of operations of designed displacement amplification mechanism is described and it is verified by using Solidworks as a simulator. Hydrodynamic resistance modeling of the device with moving valve is done for characterization of fluid flow in microfluidic channel of the device. Verification of this model is also done by using COMSOL Multiphysics CAD tool which uses finite element modeling (FEM) to make simulations.

In Chapter 3, fabrication methods, which are photolithography, electrochemical etching, wet etching, hot embossing, thermo-compression bonding and, laser micromachining, are illustrated. Due to coefficient of thermal expansion difference between the steel and the PMMA, PMMA is changed with the PEN in order to solve the integration problem of the device. Besides with the CTE match with the stainless steel, PEN is a material that has better mechanical and optical properties than PMMA. It also has a resistance to many solvents such as isopropyl alcohol (IPA) or acetone. These

specifications provide convenience of using it for fabricating microfluidic devices.

In Chapter 4, characterization of the electrochemical etching process, displacement measurements of steel displacement amplifier and, the measurement of CTE difference between the steel and the PMMA is presented. Dimensional measurements of steel displacement amplifiers fabricated in the same batch are evaluated statistically. The results show that it is possible to fabricate devices with the minimum feature size of 20μm, if undercut effect and the electrical field density distribution in considered. The displacement measurements of steel displacement amplifier show that the fabricated device can be actuated by applying simple force as deducted from the simulations of it. With the CTE measurements, it is verified that the reason of the integration problem between the steel and the PMMA plates is CTE difference.

The fluid flow measurements of the device could not be presented in this thesis because the steel displacement amplifier integrated to the PEN film with the engraved microfluidic channel on it cannot be actuated. The reason of this problem is that finger shaped structures of the steel is squeezed by PEN films after bonding and device cannot move without causing deformation on the steel beams or microfluidic channel.

As a future work, this problem of actuation after integration can be solved by developing an annealing process. In the short term, the frequency modes of vibration of the device can be found by making FEM simulations. Then, the frequency which device is vibrating in the direction of the amplified displacement can be applied. At the same time, device should be heated above the glass transition temperature of the PEN. In this way, steel fingers can be released and they can engrave their own motion path without damaging microfluidic channel. This annealing process may solve this problem.

After obtaining the device with steel trapping mechanism can be actuated by applying force, the total system can be optimized for cell culturing and analysis applications. In addition, the direct integration of steel in the microfluidic channel provides opportunity to use these trapping mechanisms to be used as electrodes. Moreover, the

information and the experience acquired from this study can help to fabricate different kinds of microfluidic devices. Also, using PEN films in these devices can speed up the development processes of these devices. In this context, this thesis can be considered as a preliminary work for developing practical microfluidic devices with using cheaper and faster fabrication methods.

REFERENCES

1. Manz, A., N. Graber and H. Widmer, "Miniaturized Total Chemical Analysis Systems: A Novel Concept for Chemical Sensing", *Sensors and Actuators B: Chemical*, Vol. 1, No. 1–6, pp. 244 – 248, 1990.

2. Whitesides, G. M., "The Origins and the Future of Microfluidics", *Nature*, Vol. 442, No. 7101, pp. 368–373, 2006.

3. Verpoorte, E. and N. de Rooij, "Microfluidics Meets MEMS", *Proceedings of the IEEE*, Vol. 91, No. 6, pp. 930–953, 2003.

4. Haeberle, S. and R. Zengerle, "Microfluidic Platforms for Lab-on-a-chip Applications", *Lab Chip*, Vol. 7, pp. 1094–1110, 2007.

5. Dittrich, P. S. and A. Manz, "Lab-on-a-chip: Microfluidics in Drug Discovery", *Nat Rev Drug Discov*, Vol. 5, No. 3, pp. 210–218, 2006.

6. Stone, H., A. Stroock and A. Ajdari, "Engineering Flows in Small Devices", *Annual Review of Fluid Mechanics*, Vol. 36, No. 1, pp. 381–411, 2004.

7. Burns, M. A., B. N. Johnson, S. N. Brahmasandra, K. Handique, J. R. Webster, M. Krishnan, T. S. Sammarco, P. M. Man, D. Jones, D. Heldsinger, C. H. Mastrangelo and D. T. Burke, "An Integrated Nanoliter DNA Analysis Device", *Science*, Vol. 282, No. 5388, pp. 484–487, 1998.

8. Manz, A., D. Harrison, E. M. Verpoorte, J. Fettinger, A. Paulus, H. Lüdi and H. Widmer, "Planar Chips Technology for Miniaturization and Integration of Separation Techniques into Monitoring Systems: Capillary Electrophoresis on a Chip", *Journal of Chromatography A*, Vol. 593, No. 1–2, pp. 253 – 258, 1992.

9. Harrison, D. J., K. Fluri, K. Seiler, Z. Fan, C. S. Effenhauser and A. Manz, "Mi-

cromachining a Miniaturized Capillary Electrophoresis-Based Chemical Analysis System on a Chip", *Science*, Vol. 261, No. 5123, pp. 895–897, 1993.

10. Hansen, C. L., E. Skordalakes, J. M. Berger and S. R. Quake, "A Robust and Scalable Microfluidic Metering Method that Allows Protein Crystal Growth by Free Interface Diffusion", *Proceedings of the National Academy of Sciences*, Vol. 99, No. 26, pp. 16531–16536, 2002.

11. Simpson, P. C., D. Roach, A. T. Woolley, T. Thorsen, R. Johnston, G. F. Sensabaugh and R. A. Mathies, "High-throughput Genetic Analysis Using Microfabricated 96-sample Capillary Array Electrophoresis Microplates", *Proceedings of the National Academy of Sciences of the United States of America*, Vol. 95, No. 5, pp. 2256–2261, 1998.

12. Liu, S., Y. Shi, W. W. Ja and R. A. Mathies, "Optimization of High-Speed DNA Sequencing on Microfabricated Capillary Electrophoresis Channels", *Analytical Chemistry*, Vol. 71, No. 3, pp. 566–573, 1999.

13. Wainright, A., U. T. Nguyen, T. Bjornson and T. D. Boone, "Preconcentration and Separation of Double-stranded DNA Fragments by Electrophoresis in Plastic Microfluidic Devices", *Electrophoresis*, Vol. 24, No. 21, pp. 3784–3792, 2003.

14. Andersson, H. and A. van den Berg, "Microfluidic Devices for Cellomics: A Review", *Sensors and Actuators B: Chemical*, Vol. 92, No. 3, pp. 315–325, 2003.

15. van den Berg, A. and T. Lammerink, "Micro Total Analysis Systems: Microfluidic Aspects, Integration Concept and Applications", A. Manz and H. Becker (Editors), *Microsystem Technology in Chemistry and Life Science*, Vol. 194 of *Topics in Current Chemistry*, pp. 21–49, Springer Berlin Heidelberg, 1998.

16. Laboratories, S. N., *Pac-Man-like Microstructure Interacts with Red Blood Cells*, 2001, `http://www.sandia.gov/media/NewsRel/NR2001/gobbler.htm`, [Accessed June 2015].

17. Unger, M. A., H.-P. Chou, T. Thorsen, A. Scherer and S. R. Quake, "Monolithic Microfabricated Valves and Pumps by Multilayer Soft Lithography", *Science*, Vol. 288, No. 5463, pp. 113–116, 2000.

18. Thorsen, T., S. J. Maerkl and S. R. Quake, "Microfluidic Large-Scale Integration", *Science*, Vol. 298, No. 5593, pp. 580–584, 2002.

19. Yamahata, C., F. Lacharme, Y. Burri and M. A. Gijs, "A Ball Valve Micropump in Glass Fabricated by Powder Blasting", *Sensors and Actuators B: Chemical*, Vol. 110, No. 1, pp. 1 – 7, 2005.

20. Choi, J.-W., K. W. Oh, J. H. Thomas, W. R. Heineman, H. B. Halsall, J. H. Nevin, A. J. Helmicki, H. T. Henderson and C. H. Ahn, "An Integrated Microfluidic Biochemical Detection System for Protein Analysis with Magnetic Bead-based Sampling Capabilities", *Lab Chip*, Vol. 2, pp. 27–30, 2002.

21. Liu, X. and S. Li, "An Electromagnetic Microvalve for Pneumatic Control of Microfluidic Systems", *Journal of Laboratory Automation*, Vol. 19, No. 5, pp. 444–453, 2014.

22. Goll, C., W. Bacher, B. Büstgens, D. Maas, R. Ruprecht and W. K. Schomburg, "An Electrostatically Actuated Polymer Microvalve Equipped with a Movable Membrane Electrode", *Journal of Micromechanics and Microengineering*, Vol. 7, pp. 224–226, 1997.

23. van der Wijngaart, W., H. Ask, P. Enoksson and G. Stemme, "A High-stroke, High-pressure Electrostatic Actuator for Valve Applications", *Sensors and Actuators A: Physical*, Vol. 100, No. 2–3, pp. 264 – 271, 2002.

24. Shikida, M., K. Sato, S. Tanaka, Y. Kawamura and Y. Fujisaki, "Electrostatically Driven Gas Valve with High Conductance", *Microelectromechanical Systems, Journal of*, Vol. 3, No. 2, pp. 76–80, 1994.

25. Liu, R. H., J. Bonanno, J. Yang, R. Lenigk and P. Grodzinski, "Single-use, Thermally Actuated Paraffin Valves for Microfluidic Applications", *Sensors and Actuators B: Chemical*, Vol. 98, No. 2–3, pp. 328 – 336, 2004.

26. Rich, C. and K. Wise, "A High-flow Thermopneumatic Microvalve with Improved Efficiency and Integrated State Sensing", *Microelectromechanical Systems, Journal of*, Vol. 12, No. 2, pp. 201–208, 2003.

27. Shao, P., Z. Rummler and W. K. Schomburg, "Polymer Micro Piezo Valve with a Small Dead Volume", *Journal of Micromechanics and Microengineering*, Vol. 14, No. 2, pp. 305–309, 2004.

28. Li, H., D. Roberts, J. Steyn, K. Turner, O. Yaglioglu, N. Hagood, S. Spearing and M. Schmidt, "Fabrication of a High Frequency Piezoelectric Microvalve", *Sensors and Actuators A: Physical*, Vol. 111, No. 1, pp. 51 – 56, 2004.

29. Goettsche, T., J. Kohnle, M. Willmann, H. Ernst, S. Spieth, R. Tischler, S. Messner, R. Zengerle and H. Sandmaier, "Novel Approaches to Particle Tolerant Valves for Use in Drug Delivery Systems", *Sensors and Actuators A: Physical*, Vol. 118, No. 1, pp. 70 – 77, 2005.

30. Yaralioglu, G. G., I. O. Wygant, T. C. Marentis and B. T. Khuri-Yakub, "Ultrasonic Mixing in Microfluidic Channels Using Integrated Transducers", *Analytical Chemistry*, Vol. 76, No. 13, pp. 3694–3698, 2004.

31. Kohl, M., D. Dittmann, E. Quandt and B. Winzek, "Thin Film Shape Memory Microvalves with Adjustable Operation Temperature", *Sensors and Actuators A: Physical*, Vol. 83, No. 1–3, pp. 214 – 219, 2000.

32. Weibel, D. B., M. Kruithof, S. Potenta, S. K. Sia, A. Lee and G. M. Whitesides, "Torque-Actuated Valves for Microfluidics", *Analytical Chemistry*, Vol. 77, No. 15, pp. 4726–4733, 2005.

33. Oh, K. W. and C. H. Ahn, "A Review of Microvalves", *Journal of Micromechanics and Microengineering*, Vol. 16, No. 5, pp. R13–R39, 2006.

34. Tsao, C.-W. and D. DeVoe, "Bonding of Thermoplastic Polymer Microfluidics", *Microfluidics and Nanofluidics*, Vol. 6, No. 1, pp. 1–16, 2009.

35. Brown, L., T. Koerner, J. H. Horton and R. D. Oleschuk, "Fabrication and Characterization of Poly(methylmethacrylate) Microfluidic Devices Bonded Using Surface Modifications and Solvents", *Lab Chip*, Vol. 6, pp. 66–73, 2006.

36. Zhang, Z., P. Boccazzi, H.-G. Choi, G. Perozziello, A. J. Sinskey and K. F. Jensen, "Microchemostat-microbial Continuous Culture in a Polymer-based, Instrumented Microbioreactor", *Lab Chip*, Vol. 6, pp. 906–913, 2006.

37. Parkinson, M. B., B. D. Jensen and K. Kurabayashi, "Design of Compliant Force and Displacement Amplification Micro-mechanisms", *Design Engineering Technical Conferences*, Vol. 37, 2001.

38. Lobontiu, N. and E. Garcia, "Analytical Model of Displacement Amplification and Stiffness Optimization for a Class of Flexure-based Compliant Mechanisms", *Computers & Structures*, Vol. 81, No. 32, pp. 2797 – 2810, 2003.

39. Yilmaz, C. and G. M. Hulbert, "Theory of Phononic Gaps Induced by Inertial Amplification in Finite Structures", *Physics Letters A*, Vol. 374, No. 34, pp. 3576 – 3584, 2010.

40. Liu, A., J. Li, Z. Liu, C. Lu, X. Zhang and M. Wang, "Self-Latched Micromachined Mechanism With Large Displacement Ratio", *Microelectromechanical Systems, Journal of*, Vol. 15, No. 6, pp. 1576–1585, 2006.

41. Gokdel, Y. D., S. Mutlu and A. D. Yalcinkaya, "Self-terminating Electrochemical Etching of Stainless Steel for the Fabrication of Micro-mirrors", *Journal of Micromechanics and Microengineering*, Vol. 20, No. 9, p. 095009, 2010.

42. Jeżowski, P., M. Nowicki, M. Grzeszkowiak, R. Czajka and F. Béguin, "Chemical Etching of Stainless Steel 301 for Improving Performance of Electrochemical Capacitors in Aqueous Electrolyte", *Journal of Power Sources*, Vol. 279, pp. 555 – 562, 2015.

43. Klank, H., J. P. Kutter and O. Geschke, "CO2-laser Micromachining and Back-end Processing for Rapid Production of PMMA-based Microfluidic Systems", *Lab Chip*, Vol. 2, pp. 242–246, 2002.

44. P P Shiu, M. O., G K Knopf and S. Nikumb, "Rapid Fabrication of Tooling for Microfluidic Devices via Laser Micromachining and Hot Embossing", *Journal of Micromechanics and Microengineering*, Vol. 18, No. 2, p. 025012, 2008.